Earth Surf. Dynam. Discuss., https://doi.org/10.5194/esurf-2019-8
Manuscript under review for journal Earth Surf. Dynam.
Discussion started: 27 February 2019

Earth Surface Dynamics Discussions
Open Access
EGU

Experiments on patterns of alluvial cover and bedrock erosion in a meandering channel

Roberto Fernández[1], Gary Parker[1,2], Colin P. Stark[3]

[1]Ven Te Chow Hydrosystems Laboratory, Department of Civil and Environmental Engineering, University of Illinois at Urbana-Champaign, Urbana, IL 61801, USA
[2]Department of Geology, University of Illinois at Urbana-Champaign, Urbana, IL 61801, USA
[3]Lamont Doherty Earth Observatory, Columbia University, Palisades, NY 10964, USA

Correspondence to: Roberto Fernández (fernan25@illinois.edu)

Abstract.

In bedrock rivers, erosion by abrasion is driven by sediment particles that strike bare bedrock while traveling downstream with the flow. If the sediment particles settle and form an alluvial cover, this mode of erosion is impeded by the protection offered by the grains themselves. Channel erosion by abrasion is therefore related to the amount and pattern of alluvial cover, which are functions of sediment load and hydraulic conditions, and which in turn are functions of channel geometry, slope and sinuosity. This study presents the results of alluvial cover experiments conducted in a meandering channel flume of high fixed sinuosity. Maps of quasi-instantaneous alluvial cover were generated from time-lapse imaging of flows under a range of below-capacity bedload conditions. These maps were used to infer patterns of particle impact frequency and likely abrasion rates. Results from eight such experiments suggest that: (i) abrasion through sediment particle impacts is driven by fluctuations in alluvial cover due to the movement of freely-migrating bars, (ii) patterns of potential erosion are functions of sediment load and local curvature, (iii) low sediment supply ratios are associated with regions of potential erosion located closer to the inner bank but this region moves toward the outer bank as sediment supply increases, and (iv) the threads of high erosion rates are located at the tow of the alluvial bars, just where the alluvial cover reaches an optimum for abrasion rate.

1 Introduction

In his report on the geology of the Henry Mountains, Gilbert (1877) described that the process of mechanical erosion of a bedrock river bed by material transported by the current depends on the hardness of the bedrock, the hardness, size and number of particles in transport, and the velocity of the stream. He noted that the number of sediment particles striking the bed and eroding it could increase up to the sediment transport capacity of the stream. At this point, the bed would be so crowded with particles that instead of colliding against the bed, they would collide against each other and the bedrock would be protected from erosion. Based on this observation, Gilbert (1877) stated that it is probable that the maximum work of mechanical erosion is performed when the load is far below the transport capacity of the stream.

During the last two decades, particular attention to the previously-described phenomenon has motivated experimental (e.g. Mishra et al., 2018; Hodge et al., 2016; Hodge and Hoey, 2016; Johnson and Whipple, 2010, 2007; Chatanantavet and Parker, 2008; Finnegan et al. 2007; Sklar and Dietrich, 1998), theoretical or numerical (e.g. Turowski 2018; Turowski and Hodge, 2017; Zhang et al. 2015; Inoue et al. 2014; Johnson 2014; Nelson et al. 2014; Nelson and Seminara, 2012; Lague, 2010; Chatanantavet and Parker, 2009; Turowski et al., 2007; Whipple et al., 2000), and field (e.g. Ferguson et al., 2017; Beer et al. 2017, 2016; Beer and Turowski, 2015; Johnson and Finnegan, 2015; Inoue et al. 2014; Cook et al., 2013, 2009; Hodge et al., 2011) work examining the relation between sediment supply, degree of alluviation, and bedrock incision in mixed bedrock-alluvial rivers. Although Gilbert (1877) did not specifically used the terms 'tools' and 'cover' effects, he described them vividly. Saltating bedload particles in a bedrock river are one of the 'tools' needed to cause incision. As sediment supply increases to a river reach, the ability to incise eventually decays due to the appearance of sediment deposits which protect the bed from further abrasion ('cover' effect). Therefore, in order for bedrock erosion to occur, a balance must exist between the 'cover' and 'tools' effects such that there are enough sediment particles in the system striking the bed, but not so many as to cover it and protect it from abrasion.

The experimental work of Sklar and Dietrich (2001, 1998) has led to a better understanding of the 'tools' and 'cover' effects. In their work, the 'tools' and 'cover' effects were parameterized in terms of a cover factor p_c which represents the areal fraction of bedrock that is covered by sediment. The exposed fraction is thus defined as $p_o = 1 - p_c$. The cover saltation-abrasion model of Sklar and Dietrich (2004) was the first to include these effects in a bedrock erosion model. The cover model used by Sklar and Dietrich (2006, 2004) to compute erosion, linearly relates the areal fraction of the bed that is covered by sediment to the ratio of sediment supply to sediment transport capacity of a bed fully covered with alluvium. The linear cover model has under certain conditions been validated via experimentation (e.g. Chatanantavet and Parker, 2008; Finnegan et al., 2007; Johnson and Whipple, 2010, 2007). Turowski et al. (2007) proposed an exponential cover model that accounts for areas of the bed with static (permanent) and dynamic (transient) cover, but their approach has not been confirmed experimentally. Lague (2010) also proposed a bedrock incision model based on stochastic variations of discharge and sediment supply which accounts for alluvial thickness and its effect on limiting bedrock incision.

Recently Zhang et al. (2018, 2015) proposed the macro-roughness saltation-abrasion alluviation model which treats the cover factor as the ratio between the alluvial thickness at a river cross section to the characteristic macro-roughness height of the bedrock surface. The approach was successfully implemented to model the evolution of bedrock river profiles. Its advantage over the original formulation is that by relating cover to alluvial thickness rather than sediment supply, it can deal with waves of alluviation and bed stripping and their dynamic effect on incision or the cessation thereof due to complete alluvial cover. Turowski (2018) presents a model that links alluvial cover to the width, slope and sinuosity of mixed bedrock alluvial rivers and postulates that change in channel width and sinuosity over time depends only on the amount of alluvial bed cover. Finally, Mishra et al. (2018) conducted experiments in a U-shaped meandering channel with constant curvature and showed that: i) lateral erosion increases with sediment supply ratio, ii) vertical incision initially grows with sediment supply but shows a more

complex relation due to the interplay between bedrock erosion and sediment deposition, and iii) zones of erosion along the tow of the point bar result in the formation of outer bedrock benches.

In spite of these developments, the cover factor definitions used so far by the different authors lack one or more important aspects required for the development of a model of bedrock incision in mixed bedrock-alluvial meandering rivers, namely:

(i) What is the role of sediment supply and local curvature and how do they affect the areas of potential erosion in meandering bedrock-alluvial channels? With the exception of the recent work by Mishra et al. (2018), Inoue et al. (2017, 2016) and Nelson et al. (2014), all models of bedrock incision by abrasion are either '0D' or '1D' and all experiments have been conducted in straight channels (Johnson and Whipple, 2010, 2007; Chatanantavet and Parker, 2008; Finnegan et al., 2007). There is still no baseline set of experiments describing how the pattern of spatial cover is established in a meandering channel, and how it varies with local curvature and sediment supply.

(ii) What is the appropriate averaging window to characterize the areal fraction of alluvial cover? The model based on the areal fraction of cover uses an average value defined over an "appropriate" averaging window, but only loose definitions regarding its length scale and timescale have been provided to date. Moreover, this mean cover value assumes that the alluvial deposits covering the bed are transient. Field observations (Inoue et al. 2014, Cook et al. 2013, 2009) and laboratory experiments (Johnson and Whipple, 2010, 2007; Chatanantavet and Parker, 2008; Finnegan et al., 2007) indicate that zones of permanent cover and permanent exposure coexist with transient deposits in mixed bedrock-alluvial rivers.

(iii) What is the role of alluvial cover fluctuations on erosion? Current models rely on a mean cover value, but temporal alluvial cover fluctuations provide a better representation of the frequency of the saltating bedload particle impacts on the bed which are responsible for bedrock erosion.

We addressed these questions by conducting experiments in a high-amplitude laboratory meandering flume to characterize the statistics of alluvial cover as they relate to the sediment supply ratio and local curvature. The materials and methods for the experiments are described in Sec. 2. Section 3 presents the results of the experiments, and is followed by the discussion (Sec. 4) and conclusions (Sec. 5). To close this introductory section, a summary of relevant concepts is provided.

1.1 Bedrock erosion and alluvial cover

The time rate of bedrock incision (erosion) by mechanical wear E_s has been quantified with Eq. 1 by different authors (e.g. Sklar and Dietrich, 2004, 2006; Turowski et al., 2007; Chatanantavet and Parker, 2009) as follows;

$$E_s = V_i I_r p_o \quad (1)$$

In Eq. 1, V_i is the volume of bedrock lost per particle impact, I_r is the particle impact rate per unit area per unit time and p_o is the fraction of exposed bedrock. The areal fraction of alluvial cover, i.e. cover factor p_c is thus defined as $p_c = 1 - p_o$. An alternative but closely related equation to compute erosion is presented in Eq. 2 (e.g. Turowski et al., 2008; Chatanantavet and

Earth Surf. Dynam. Discuss., https://doi.org/10.5194/esurf-2019-8
Manuscript under review for journal Earth Surf. Dynam.
Discussion started: 27 February 2019

Parker, 2009) where β is a parameter that relates to the fraction of bedrock volume that is lost per particle impact at the end of each saltation, q_{bt} is the capacity bedload transport rate per unit width for a bed fully covered with alluvium, and $q_{bs} = p_c q_{bt}$ is the actual bedload transport rate per unit width given that transport can only occur over the portion of the bed that has an alluvial cover.

$$E_s = \beta q_{bs} p_o = \beta q_{bt} p_c (1 - p_c) \tag{2}$$

In Sklar and Dietrich (2004) and other works based in their cover model (e.g. Turowski et al., 2007; Lamb et al., 2008), p_o represents the areal fraction of exposed bedrock. In the Zhang et al. (2015) cover model, p_o also represents the fraction of bed elevation at a given cross section which is not covered by alluvium, but is instead related to the ratio η_a / L_{mr}, where η_a is a measure of the thickness of alluvium, and L_{mr} is a measure of the intrinsic macro-roughness height of the bedrock surface itself.

Both definitions are presented schematically in Figure 1. In general, p_c is an arbitrary function of q_{bs}/q_{bt} or η_a/L_{mr}, but the simplest realistic forms are given by Eq. 3 and Eq. 4.

$$p_c = 1 - p_o = \begin{cases} \frac{q_{bs}}{q_{bt}} & if\ 0 \le \frac{q_{bs}}{q_{bt}} < 1 \\ 1 & if\ 1 \le \frac{q_{bs}}{q_{bt}} \end{cases} \tag{3}$$

$$p_c = 1 - p_o = \begin{cases} \frac{\eta_a}{L_{mr}} & if\ 0 \le \frac{\eta_a}{L_{mr}} < 1 \\ 1 & if\ 1 \le \frac{\eta_a}{L_{mr}} \end{cases} \tag{4}$$

The use of Eq. 3 or Eq. 4 in combination with Eq. 1 must be employed in terms of an appropriate averaging window over which to determine the cover fraction p_c and open fraction $p_o = 1 - p_c$. For example, Sklar and Dietrich (2006), Gasparini et al. (2007) and Chatanantavet and Parker (2008) assume, explicitly or implicitly, that a) the averaging window is at least as large as channel width, and b) that p_c fluctuates temporally between 0 and 1 within the window. If this were not the case, zones within the channel where p_c permanently takes the values 0 and 1 would never be subject to incision, and channel geometry would not change over time. However, if these assumptions are met over an appropriate time scale, all the channel along a cross-section would, in the long-term average, erode at the same rate. In the case of mixed bedrock-alluvial meandering rivers, where permanent alluvium deposits in e.g. point bars, the assumptions just described break down. In such rivers, erosion occurs only in areas with transient cover and is not expected to occur in areas that are permanently covered or exposed. Under certain conditions, specific areas of the channel might have little to no probability of being struck by sediment particles, thus limiting the areas that could undergo erosion.

Earth Surf. Dynam. Discuss., https://doi.org/10.5194/esurf-2019-8
Manuscript under review for journal Earth Surf. Dynam.
Discussion started: 27 February 2019

2 Materials and Methods

2.1 Flume

Experiments were conducted in the Kinoshita Flume at the Ven Te Chow Hydrosystems Laboratory, University of Illinois at Urbana-Champaign. The flume, shown in Fig. 2b, is 0.60 m wide, 0.40 m deep and 36 m long (along the centerline including upstream and downstream tanks), and has a sinuosity of 3.7. All three meander bends are identical and have a down-channel wavelength of 10 m. All results presented herein correspond to experiments conducted with water flowing from right to left as indicated in Fig. 2c, i.e. with the bends skewed in the upstream direction. Readers interested in more specific details about the Kinoshita flume are referred to Abad and Garcia (2009a, b).

2.2 Bed-material properties and bed characteristics

The bed material used in the experiments was crushed walnut shells, which have a specific gravity in the range 1.3-1.4. A bedrock basement was built in the flume using the bathymetry measured by Czapiga (2013), who conducted experiments under fully alluvial conditions using the crushed walnut shells. After averaging out the bedforms, the transverse slopes every 0.5 m were calculated. Based on them, foam cross-sections were cut and placed inside the flume. Pea gravel was used to fill the flume following the profile established by the foam. The size of the gravel was chosen so as to prevent it from being transported by the flow in the experiments. The region between streamwise stations CS07 and CS23 (Fig. 2c) was filled with gravel to an elevation slightly below the maximum given by the foam. This section was then covered with a ~ 1 cm layer of concrete and used to create the bedrock surface. Figure 3c shows the bedrock bed built inside the Kinoshita Flume, and Fig. 2a shows its bathymetry. The concrete was painted white to enhance the contrast between the bedrock and the alluvium.

The grain size distributions of the crushed walnut shells, the pea gravel, and the dry concrete mix (including gravel, sand and cement) are shown in Figure 3a. The inset figure includes the results of laser scans conducted to measure the as-built bedrock macro-roughness.

2.3 Bed laser scans

A Keyence laser with sub-millimeter precision was used to scan the bed at five different locations, namely: CS10, CS12, CS15, CS17 and CS20 (Fig. 2c). A 4^{th} order polynomial was fit to the scans, and residual elevations were calculated by subtracting the actual reading from the polynomial. The average residual elevation along the cross sections was calculated and used to estimate the macro-roughness of the bedrock bed, defined here as the difference between the maximum and minimum elevations. The resulting value (10 mm) is also indicated in Fig. 3a.

2.4 Areal alluvial cover measurements

The percentage of areal alluvial cover was calculated by analyzing time-lapse images of the flume bed. Images were taken, on average, every 10 s (0.1 Hz) during the duration of every run and processed in Matlab. A region of interest (ROI) was selected

for each image series. In this study, the ROI corresponds to the middle bend of the Kinoshita flume, i.e. between streamwise locations 10 m and 20 m (Fig. 2).

Images were first converted to gray scale, and then the method of Otsu (1979), as implemented in Matlab ('graythresh' function), was used to make the images binary. The resulting black (alluvial cover) and white (bedrock) images were used to calculate the percent areal cover. The fraction of alluvial cover was determined as shown in Eq. 5.

$$p_{c_{ROI}} = \frac{\left(N - \sum_{j=1}^{N} px_j\right)}{N} \quad (5)$$

In Eq. (5), pc_{ROI} = percent of areal alluvial cover inside the region of interest; N = total number of pixels inside the region of interest (i.e. total area); and px_j = value of the jth pixel in the binary image (white pixels are equal to one and black pixels are equal to zero). More details regarding the image acquisition and processing are included in the supplemental material (S1).

2.5 Relation between alluvial cover and sediment supply

A rectangular bedrock slab was built with the same materials used to build the bedrock basement in the flume. The bedrock slab was built over a piece of foam laid on a floor so as to have no longitudinal or transverse slope. Pea gravel was placed over the foam and a thin layer of concrete was poured over it. It was then painted white to increase contrast between the bedrock and the alluvium. The purpose of this bedrock slab, which was 0.6 m long by 0.4 m wide, was to measure i) the relation between areal alluvial cover and sediment supply ratio, and ii) the relation between areal alluvial cover and the ratio of alluvial cover thickness to bedrock macro-roughness.

To quantify the sediment supply ratio, known weights of sediment were incrementally added to the slab and spread evenly until the bed was fully covered with alluvium. Eleven iterations were necessary to cover the bed completely. The sediment supply ratio was calculated as the cumulative weight of sediment in every iteration, divided by the total weight of sediment used to fully cover the bed. Areal alluvial cover was quantified using images, and following the approach described in section 2.4. The ratio of alluvial cover thickness to bedrock macro-roughness was quantified by scanning nine cross sections of the bedrock slab with a sub-millimeter precision Keyence laser. The cross sections were 4 cm away from each other. The first set of scans were conducted over the bare bedrock slab, and then they were repeated each time that alluvium was added over the slab. The entire process was conducted two times to mitigate any human induced errors in the measurements. After the first set of measurements, the alluvium was removed with a brush first and then with an air-pressure hose to make sure all grains were removed from the slab.

2.6 Experimental conditions

Table 1 shows the general experimental conditions used in this study. The flow discharge rate used in all runs was 12.3 liters per second (Ls^{-1}) which corresponds to the flow rate used by Czapiga (2013). This flow rate created the alluvial bathymetry

used to build the bedrock bed in this experiments. The flow discharge was measured with electromagnetic flow meters. Given that the sediment recirculating pump only works at a constant discharge of 3.1 Ls^{-1}, the main pump was set to have a discharge of 9.2 Ls^{-1}.

The volume of sediment inside the Kinoshita flume was modified between runs so as to obtain different reach-averaged areal ratios of alluvial cover. Runs in this study are identified based on this value (Table 2). For example, run "pc79" had 79% of the total bed area covered with alluvium after averaging in space (one wavelength) and time (one hour). The first run conducted was pc79, followed by pc72 and pc54. Afterwards, all the sediment was removed from the system to run the bare-bedrock condition, pc00. The following runs were pc19, pc27, pc38 and pc46, conditions that were achieved after progressively adding sediment to the flume.

Water surface slopes were initially calculated by using the water level elevation changes in the upstream and downstream tanks of the Kinoshita flume. Both tanks have a measuring tape glued to the upstream- and downstream-most walls (Fig. 2b). These measuring tapes were used to guarantee that runs always started at the desired water elevation. Before turning on the pumps, desired water elevations were verified, and after the run had started, readings were taken every 20-30 minutes.

Water surface elevations were also measured with eTapes in runs pc00, pc19, and pc79 (Fernández, 2018). An eTape is a sensor with a resistive output that varies with the level of fluid in which it is immersed. The resistive output of the sensor is inversely proportional to the height of the water. Low water depths correspond to high output resistance. Conversely, high water depths correspond to low output resistance. Details about the eTape installation, calibration, and operation are given in S2, and further information may be found in Fernández (2018). After runs pc79, pc72 and pc54 were finished, we noticed that the water surface slopes in the Kinoshita flume were different depending on if they were calculated for the total length of the flume, i.e. between tanks, or for the middle bend of the flume only. Figure 4 shows an example of the water surface elevations measured with the eTapes (middle zone of flume) and the measuring tapes (entire flume) for run pc79. To accurately measure the middle bend water surface slopes in runs pc00-pc46, point gages were placed on the flume at streamwise locations 9 m and 21 m (Fig. 2). The slopes calculated with the point gage readings are shown in Table 1. The average ratio of the slopes calculated with the point gages to those calculated with tank elevations in runs pc00 – pc46 was used to estimate the slopes in the middle bend of the flume for runs pc54, pc72 and pc79.

The sediment transport rates were measured by collecting material in the sediment trap located at the upstream end of the flume (Abad and Garcia, 2009b). Average values are shown in Table 2.

3 Results

3.1 Relation between alluvial cover and sediment supply

Figure 5a shows the relation between areal alluvial cover and sediment supply ratio measured on the bedrock slab. Figure 5b shows the relation between areal alluvial cover and the ratio of alluvial cover thickness to bedrock macro-roughness measured

on the bedrock slab. The thin dashed lines with circle markers show the average results of the measurements; the thick dashed lines correspond to a best-fit line; and the dotted lines show the linear relation between variables that has been used by previous authors (e.g. Inoue et al., 2016, 2014; Zhang et al., 2018, 2015; Chatanatavet and Parker, 2009, 2008; Sklar and Dietrich, 2006, 2004). Figure 5c shows the relation between reach-averaged alluvial cover (spatial average measured over one wavelength) and sediment supply ratio measured in the Kinoshita flume. Figure 6 shows a snapshot of the middle bend of the Kinoshita flume corresponding to each one of the eight reach-averaged alluvial cover conditions. Links to the videos showing the bed evolution for the different experimental conditions are included in the 'Video supplement' section at the end of the paper.

3.2 Reach averages of alluvial cover fraction

Figure 7 shows the reach-averaged temporal series of areal alluvial cover for the seven experiments with alluvium. Figure 8 shows the maps of alluvial cover for all experimental conditions. Therein, black areas show regions that were permanently covered with alluvium; white areas show regions of permanently exposed bedrock; and colored regions show areas that were covered with alluvium for a fraction of the time.

3.3 Regions with transient alluvial cover

The alluvial cover maps in Figure 8 show different percentages of permanently covered or exposed bedrock, as well as regions with transient alluvial cover. To delineate and quantify these areas, the following criteria were used: regions with permanent alluvial cover are those in which $p_c > 0.975$; regions with permanent exposed bedrock are those in which $p_c < 0.025$; and regions with transient alluvial cover are those in which $0.025 \leq p_c \leq 0.975$. Using these criteria, maps of transient alluvial cover were prepared. Figure 9 shows the regions of transient cover (gray), permanent cover (black) and permanently exposed bedrock (white) for each of the eight experimental conditions.

Figure 10 shows the reach-averaged percentages of these three regions for all eight experimental conditions. Therein, the yellow dashed line corresponds to the reach-averaged fraction of permanently exposed bedrock; the blue line corresponds to the reach-averaged fraction of permanently covered bedrock; the light-blue line corresponds to the reach-averaged fraction of the bed with transient cover; the thick black line corresponds to the sum of the transient and permanent cover fractions; and the black dotted line corresponds to the 1:1 line.

3.4 Cross-section averages of alluvial cover

Figure 11 shows the cross-sectional alluvial cover averages for the seven experimental conditions with alluvium. Values were extracted every meter between streamwise locations 10 m and 20 m. Therefore, eleven local alluvial cover values were obtained for each experiment. As in the case of the reach-averaged values, these results include permanently covered and exposed

portions of the cross section as well as a fraction with transient alluvial cover. Figure 12 shows the ratios of the cross sections that had permanently exposed bedrock (dashed yellow line), permanently covered bedrock (blue line), transient alluvial cover (light-blue line), and the ratio corresponding to the sum of permanent plus transient cover (black line) for all experimental conditions but pc00.

Cross section alluvial cover values were normalized with the reach-averaged value. Figure 13 shows boxplots with the results. The dimensionless curvature of the Kinoshita flume is also plotted. The boxes include information at each cross section for the seven experiments. The median value is indicated by the red line inside the box; the bottom line on each box corresponds to the first quartile (q_1); the top line on each box corresponds to the third quartile (q_3); whiskers extend to $q_1 - 1.5(q_3 - q_1)$ at the bottom and $q_3 + 1.5(q_3 - q_1)$ at the top; and values lying outside this range are considered outliers and are indicated with a red cross.

3.5 Erosion potential based on alluvial cover averages

Based on Eq. 2, a dimensionless erosion potential E_{sp} may be expressed as shown in Eq. 6 below. Figure 14 shows the erosion potential for all experimental conditions. The regions with the largest erosion potential are shown in blue whereas the regions with no erosion potential are shown in white.

$$E_{sp} = p_c(1 - p_c) \tag{6}$$

4 Discussion

4.1 Relation between alluvial cover and sediment supply

Figure 5a shows the relation between alluvial cover and sediment supply ratio for the bedrock slab and Fig. 5c shows it for the Kinoshita flume. Both relations obtained in this study are logarithmic (Eq. 7). The value of the constant 'a' is different between the bedrock slab (a =0.23) and the Kinoshita flume (a = 0.14) but the shape of the relation is the same. Previous research has shown that a linear relation between percent cover and sediment supply ratio is valid under certain circumstances (e.g. Inoue et al, 2014; Chatanantavet and Parker, 2008) but our results suggest that a different relation is also possible:

$$p_c = a \cdot ln\left(\frac{q_{bs}}{q_{bt}}\right) + b \tag{7}$$

In the case of the bedrock slab, the logarithmic relation suggests that, initially, the areal cover increases rapidly with sediment supply ratio. Once the smaller voids in the bed are filled, more and more alluvium is needed to fully cover the largest roughness elements and further increase p_c.

In the case of the Kinoshita flume, the logarithmic relation between alluvial cover and sediment supply ratio is believed to be due in large part to the formation of point bars and transient alluvial deposits. Initially, a small amount of alluvium covers a

Earth Surf. Dynam. Discuss., https://doi.org/10.5194/esurf-2019-8
Manuscript under review for journal Earth Surf. Dynam.
Discussion started: 27 February 2019

proportionately larger area of the bed, but as sediment supply increases, alluvial thickness growth is favored over areal extent of alluvial cover. As more alluvium accumulates over regions previously covered, additional sediment supplied to the reach tends to deposit at the edge of the existing deposits, thus increasing alluvial cover, but at an ever smaller rate.

Figure 5b shows the relation between areal alluvial cover and alluvial thickness to bedrock macro-roughness ratio. Zhang et al. (2018, 2015) and Inoue et al. (2014) used the assumption that the relation is linear but the results obtained for the bedrock slab suggest that an 'S-shaped' (sigmoid curve) relation is more appropriate. A logistic curve, which is a type of sigmoid curve, was fit to the measurements in this study. Eq. 8 shows the general logistic function and Eq. 9 shows the one used here. Comparing the two, it may be seen that: $x = \eta_a/L_{mr}$; $f(x) = p_c(\eta_a/L_{mr})$; L is the maximum value of the curve, corresponding to $p_{c_{max}} = 1.0$; k is the steepness of the curve; and x_o is the x-value of the sigmoid curve's midpoint. As shown in Figure 5b and Eq. 9, the steepness used to fit the sigmoid curve to the measured values was 8 and the midpoint was defined at $\eta_a/L_{mr} = 0.4$.

It is likely that the steepness and midpoint value are associated to some measure of the grain size distribution of the alluvium and the macro-roughness height of the bedrock. In the case of the bedrock and alluvium (Fig. 3a) used in this study, the steepness value corresponds to $k \sim L_{mr}/D_{16}$ and the mid-point value corresponds to $x_o \sim 2.1D_{84}/L_{mr}$. This issue merits further investigation so as to define appropriate relations to calculate the steepness and mid-point value of the sigmoid curve for implementation in numerical models.

$$f(x) = \frac{L}{1+e^{-k(x-x_o)}} \tag{8}$$

$$p_c(\eta_a/L_{mr}) = \frac{1.0}{1+e^{-8[(\eta a/L_{mr})-0.4]}} \tag{9}$$

4.2 Reach averages of alluvial cover

Figure 7 shows the temporal evolution of reach-averaged alluvial cover for all experimental runs. Larger fractions of alluvial cover are associated with fluctuations about the mean value due to the appearance of freely-migrating bars as sediment supply increases. Figure 8 shows the maps of alluvial cover for all experimental runs. Darker shades of blue correspond to areas that were covered with alluvium for more than 70% of the time; and shades of yellow correspond to areas that were covered with alluvium less than 30% of the time. In regards to the 'tools' and 'cover' effects, the white and black regions in those alluvial cover maps would not experience erosion. No tools (alluvium) are available to erode the bed in the white regions whereas alluvium completely covered the bed in the black regions, thus protecting it from erosion.

The areal alluvial cover definition in Fig 1a is based on the assumption that alluvial deposits are transient, i.e. no portions of the bed in the reach remain permanently covered with alluvium or fully exposed. This assumption is not met in meandering channels where permanent alluvial cover deposits form and grow as sediment supply increases, and erosion may only occur in those regions where alluvial cover is changing in time, i.e. regions with transient cover.

Earth Surf. Dynam. Discuss., https://doi.org/10.5194/esurf-2019-8
Manuscript under review for journal Earth Surf. Dynam.
Discussion started: 27 February 2019

4.3 Regions of transient alluvial cover

The regions of transient alluvial deposits are those over which alluvial cover is changing in time (colored regions in Fig. 8). Figure 9 shows the regions of transient alluvial cover in gray, regions of permanent alluvial cover in black and regions of permanently exposed bedrock in white. The area of the former two regions increases with sediment supply, whereas the area of the latter decreases as sediment supply increases. Figure 10 shows the growth of the regions of permanent and transient cover as a function of reach-averaged alluvial cover. The regions of permanently exposed bedrock decrease accordingly. In general, both the fraction of the total area with permanent and transient cover grow at a similar rate with increasing reach-averaged p_c. The reach-averaged conditions for which transient and permanent cover have similar area ratios are p_c = 0.27, 0.46, 0.54 and 0.72. The largest differences between permanent and transient cover are observed at p_c = 0.19, 0.38 and 0.79. The case of p_c = 0.19 is likely due to the typical sedimentation patterns observed in meandering bedrock channels when alluvial point bars first form. Immediately downstream of the bend apices, i.e. points of highest curvature, sediment is deposited. In the Kinoshita flume, the apices of bends are located at streamwise locations 9.5 m, 14.5 m and 19.5 m (Fig. 13). Initially, these locations become the upstream-most points of the point bars. Once these deposits have been established, and as long as sediment continues to be supplied from upstream, the incoming particles travel above the existing deposit due to decreased resistance from the bed. Under such conditions, permanent alluvial cover is favored over transient alluvial cover.

The case p_c = 0.38 has a larger portion of the total area with transient cover than with permanent cover. As more sediment was supplied to the system while keeping the initial water depth constant (Table 1), the alluvial thickness could not continue to grow indefinitely but rather, the areal extent of alluvial cover grew instead. Sediment particles could no longer be preferentially transported over the alluvial deposits, and began to be transported closer to the edge of the existing deposits.

The case p_c = 0.79 shows a dip in the ratio of transient cover, while the area with permanent cover continues to increase. Although there are no runs with a larger reach-averaged fraction of alluvial cover, it is likely that this trend would be maintained until the bed is completely covered with alluvium. As p_c grows, the area ratio of permanently covered regions should increase at a faster rate, and the area ratio of regions with transient cover should decrease rapidly towards zero. Eventually, the channel will not have any area left for the areal extent of alluvial cover to grow, so that further deposition promotes increased alluvial thickness instead.

The reach-averaged results shown in Fig. 8, Fig. 9 and Fig. 10 suggest that the areas subject to erosion in mixed bedrock-alluvial meandering rivers are a fraction of the total reach area. In the case of the Kinoshita flume experiments presented in this study, the areas with transient alluvial deposits occupied less than 50% of the total reach area, hence erosion could only occur within a restricted portion of total bed area.

Earth Surf. Dynam. Discuss., https://doi.org/10.5194/esurf-2019-8
Manuscript under review for journal Earth Surf. Dynam.
Discussion started: 27 February 2019

4.4 Cross-sectional averages of alluvial cover

Figure 11 shows the cross-section-averaged fraction of alluvial cover for all experimental conditions that had alluvium. Values were calculated every meter between streamwise locations 10 m and 20 m. In general, all conditions exhibit similar trends, with local lows in p_c at streamwise locations 15 m and 19 m and local highs at streamwise locations 11 m and 16 m. The regions showing higher local percentages of alluvial cover are located 1.5 m downstream of the bend apices. Point bar deposits are responsible for the higher local value of p_c at these locations. On the other hand, the local lows in p_c are associated with the points of highest curvature in the reach. Both local lows are within 0.5 m of the bend apices.

Figure 12 shows the fractions of each cross section that have permanent alluvial cover (blue line), transient alluvial cover (light-blue line), exposed bedrock (yellow dashed line), and permanent + transient cover (black line) for all experimental conditions. The ratio of exposed bedrock peaks in the vicinity of the bend apices. Even in the case of reach-averaged $p_c = 0.79$, portions of the bed in these areas remain exposed due to high curvature. Except for the cases with reach-averaged $p_c = 0.38$ and 0.54, no cross sections have fractions with transient alluvial cover greater than 60%.

The average fractions of transient alluvial cover at the cross-sectional level have values of 0.10 for $p_c = 0.19$, 0.21 for $p_c = 0.27$ and between 0.31 and 0.34 for the other experimental conditions. In spite of the local variations in transient alluvial cover, potential erosion is, on average, limited to a rather small portion of the cross section. This is likely due to the combined effects of sediment supply ratio and local curvature.

Figure 12 shows box plots of cross-sectionally averaged p_c normalized with the reach-averaged value. The figure also shows the dimensionless curvature of the Kinoshita flume (black dashed line), the negative value of the curvature (gray dotted line) and the median normalized values of p_c (red line). The true (κ) and negative ($-\kappa$) centerline curvature signals are shown to better highlight the trend of normalized p_c with curvature. The cross sections located close to the bend apices, i.e. regions with local high curvature, show normalized p_c values below unity, whereas the regions with smaller curvature values show normalized p_c values above unity. Normalized, local p_c values follow the overall trend of local curvature.

4.5 Erosion potential based on alluvial cover averages

Figure 14 shows the erosion potential (Eq. 6) for all experimental conditions. Regions with higher erosion potential are those for which alluvial cover averages were close to 0.5, in accordance with the parabolic form of Eq. 6. These regions are shown in dark blue in figure 13. White regions have no erosion potential due to a lack of tools or the presence of alluvial cover protecting the bed from abrasion. The regions of potential erosion are limited to the areas with transient alluvial cover. In general, their width is a function of sediment supply ratio, with narrower regions associated with smaller sediment supply ratios. Locally, the width of these regions is affected by curvature as well, with narrower regions in areas of high curvature, and wider regions in areas of lower curvature.

The region of potential erosion is located closer to the inner bank for lower sediment supply ratios, and moves outward as sediment supply increases. Focusing on the region of potential erosion located at the bend apex at streamwise location 14.5 m, it is seen that for $p_c = 0.27$, the region is located right next to the inside bank whereas for $p_c = 0.79$, the region is much closer to the outer bank. Figure 15 shows an image of the mixed bedrock-alluvial Shimanto River in Shikoku, Japan and a sketch of what the cross section might look like with the areas of erosion and no erosion indicated. The reach shown in the image has an alluvial point bar on the inside of the bend, a narrow inset channel at the edge of the point bar and an exposed bedrock bench on the outside of the bend. The same morphologies have been observed in a smaller scale stream called Pescadero Creek, in California, USA (Fig. 6B in Johnson and Finnegan, 2015). The experiments of Mishra et al. (2018) also show that when sediment supply is low, the alluvial point bar is narrow and an inset channel is eroded at the toe of the point bar, leaving an exposed bedrock bench on the outer part of the bend.

The typical geometry of an alluvial meandering channel cross section is shallow on the inside and deep on the outside. The reach of the Shimanto River shown in Figure 15 has a different geometry. The deepest portion of the channel is not located on the outer bank. Instead, it is located at the toe of the point bar, which happens to be approximately at the middle of the cross section. It is likely that the narrow inset channel was formed during a long period of decreased sediment supply. During this period, the region of transient alluvial cover was confined to the current width of the channel shown in the image. The outer bedrock bench could potentially be eroded if sediment supplied to the reach from upstream were to be increased, and maintained at this increased value for an extended period of time. If this occurred, the point bar would likely extend toward the outer part of the bend, thus moving the area of transient alluvial cover farther into this region.

4.6 Erosion potential based on alluvial cover fluctuations

The results of alluvial cover shown and discussed up to this point correspond with spatial or temporal averages. Nonetheless, at the microscopic level, the value of p_c can only take values of zero (exposed bedrock) or one (covered with alluvium). In the context of the areal images obtained during the experiments, this means that pixels may change between white and black throughout the run. This information was used herein to quantify erosion potential based on alluvial cover fluctuations.

Bedrock incision can only occur when a particle strikes the bed. If a pixel changes from white to black between consecutive images, it means that sediment particles traveled into the area and struck the bed. If the pixel remains black or white in consecutive images, no strikes occurred; and if the pixel changes from black to white, sediment particles have left, and thus did not strike the bed. With these definitions, the erosion potential may be quantified by counting the number of times that a pixel changes from white to black, i.e. by quantifying the fluctuations in alluvial cover.

The frequency of strikes (f_s) at the j^{th} pixel corresponds to the number of times that the j^{th} pixel has changed from white ($p_c = 0$) to black ($p_c = 1$) between consecutive images (im), divided by the total number of images (N) in the series (Eq. 10).

$$f_{s_j} = \frac{\sum_{i=1}^{N}\left(\frac{dp_C}{dim_i}=-1\right)_j}{N} \quad (10)$$

Earth Surf. Dynam. Discuss., https://doi.org/10.5194/esurf-2019-8
Manuscript under review for journal Earth Surf. Dynam.
Discussion started: 27 February 2019

Figure 16 shows the frequency of strikes (f_s) for all experimental conditions. In general, the areas in color in the figure are similar to the areas with transient alluvial cover shown in Fig. 9 and the areas with erosion potential in Fig. 14. Picking out differences in these particular figures is not straightforward, but the videos included in the supplemental material illustrate the migrating erosion fronts, and suggest that erosion is likely to be driven predominantly by the movement of freely-migrating bars. The use of the frequency of strikes associated with fluctuations in alluvial cover provides an improved approach for computing bedrock erosion by abrasion, as discussed below.

4.7 Alluvial cover fluctuations vs. averages

The use of temporal averages of alluvial cover has limitations. Figure 17 shows a hypothetical example of two cases in which the long-term average of alluvial cover is equal, but the fluctuations in alluvial cover between them are different. Given that erosion by abrasion is driven by the number of times the bed is struck by particles, erosion would only occur in the first case. Erosion would only occur each time the area changes from white to black, i.e. every time a particle moves into the area and strikes the bed upon arrival. This simple example suggests that the use of temporal averages of alluvial cover to calculate erosion may lead to inaccurate results.

The use of a relation such as Eq. 2 with spatiotemporal averages of alluvial cover also has limitations. According to it, the following experiment pairs: i) $p_c = 0.19$ and $p_c = 0.79$; ii) $p_c = 0.27$ and $p_c = 0.72$; and iii) $p_c = 0.46$ and $p_c = 0.54$ should have very similar, or equal, erosion potentials as shown below:

i) $E_{sp} = 0.19(1 - 0.19) = 0.19(0.81) = 0.154$ *and* $E_{sp} = 0.79(1 - 0.79) = 0.79(0.21) = 0.166$

ii) $E_{sp} = 0.27(1 - 0.27) = 0.27(0.73) = 0.197$ *and* $E_{sp} = 0.72(1 - 0.72) = 0.72(0.28) = 0.202$

iii) $E_{sp} = 0.46(1 - 0.46) = 0.46(0.54) = 0.248$ *and* $E_{sp} = 0.54(1 - 0.54) = 0.54(0.46) = 0.248$

Figure 14 and the videos in S3 show that the erosion potential in all cases is different, thus suggesting that spatial averaging may also lead to inaccurate results. For these reasons, temporal and spatial averages of alluvial cover are not appropriate to quantify erosion in mixed bedrock-alluvial rivers. The computational method of Inoue et al. (2016, 2017) both tracks the migration of cover fronts and bars and calculates cover at a spatiotemporally local level, thus approaching the methodology suggested here.

5 Conclusions

The results of this study lead to the following conclusions:

1. The percent of areal alluvial cover (p_c) initially grows rapidly with increasing sediment supply ratio (q_{st}/q_{bt}) in meandering channels. Rapid initial growth is likely due to the formation of point bars. Following the formation of these initial deposits, addition of more sediment into the system first promotes the growth of alluvial thickness and later promotes the growth of areal extent in alluvial cover. Therefore, a logarithmic relation between these variables reflects their relation better than a linear one. A logarithmic relation allows for rapid initial growth of p_c with increasing sediment supply ratio, but as the sediment supply ratio increases, p_c growth slows down.
2. The percent of areal alluvial cover (p_c) as a function of the ratio between alluvial thickness and bedrock macro-roughness (η_a/L_{mr}) follows an S-shaped (sigmoid) curve. A logistic curve is recommended for models of bedrock erosion that use this framework.
3. The steepness and intersection parameters needed in the logistic curve are likely functions of a characteristic grain size of the alluvium and the bedrock macro-roughness. In this study, the steepness and intersection values used were given by $k \sim L_{mr}/D_{16}$ and $x_o \sim 2.1 D_{84}/L_{mr}$ respectively.
4. Mixed bedrock-alluvial meandering channels may have areas with permanent and transient alluvial cover as well as areas of permanently exposed bedrock. Erosion by abrasion is possible only in the areas with transient alluvial cover. Local normalized p_c values are smaller than reach-averaged values at regions with high curvature and higher at regions with lower curvature.
5. The size and location of the areas of preferential erosion in mixed bedrock-alluvial meandering rivers are a function of sediment supply ratio and local curvature. Low sediment supply ratios are associated with regions of potential erosion located closer to the inner bank. This region moves toward the outer bank as sediment supply increases. High local curvature values are associated with narrow regions of potential erosion whereas lower curvature values are associated with wider regions of potential erosion.
6. The use of either spatially or temporally averaged values of p_c, or a combination of both, is not necessarily an appropriate approach to model bedrock erosion by abrasion of bedload. The largest spatial window recommended should be as small as possible so as to capture the local spatiotemporal fluctuations in alluvial cover. The longest temporal window recommended should be quasi-instantaneous so as to capture the temporal fluctuations in alluvial cover.

5.1 Future research directions

Based on the results of this study, the following two research directions are proposed:

1. Conduct experiments with the objective of determining appropriate relations to define the steepness and intersection of the sigmoid function for use in numerical models of bedrock erosion based on a framework using ratio of alluvial thickness to bedrock macro-roughness.

2. Develop a model of bedrock erosion by abrasion based on the fluctuations of areal alluvial cover. The model must take into consideration the role of freely-migrating bars and their celerity. The numerical formulation of Inoue et al. (2017, 2016) offers an important advance in this regard.

Code Availability

The Matlab routines developed to process the time lapse images and eTape data are available at https://doi.org/10.13012/B2-3044828_V1.

Data availability

All data used in preparation of this manuscript is available at https://doi.org/10.13012/B2-3044828_V1.

Video supplement

Videos showing the evolution of the bed and the erosion fronts are available at:
https://av.tib.eu/series/606/experiments+on+patterns+of+alluvial+cover+and+bedrock+erosion+in+a+meandering+channel

Author contributions

Experiments were designed by all authors. R. Fernández conducted the experiments, data analysis and post-processing. Initial manuscript was prepared by R. Fernandez and G. Parker. All authors worked on the final version submitted.

Competing interests

The authors declare that they have no conflict of interest.

Acknowledgements

Participation of all authors in this study was possible thanks to funding provided by the US National Science Foundation [grant EAR1124482]. The authors would like to thank Alejandro Vitale, PhD for his help building the eTape system, assistance with Arduino code development, and preparation of the wiring diagram.

References

Abad, J. D., and Garcia, M.H.: Experiments in a high-amplitude Kinoshita meandering channel: 1. Implications of bend orientation on mean and turbulent flow structure, Water Resour. Res., 45, W02401, https://doi.org/10.1029/2008WR007016, 2009a.

Abad, J. D., and Garcia, M.H.: Experiments in a high-amplitude Kinoshita meandering channel: 2. Implications of bend orientation on bed morphodynamics, Water Resour. Res., 45, W02402, https://doi.org/10.1029/2008WR007017, 2009b.

Beer, A. R., and Turowski, J. M.: Bedload transport controls bedrock erosion under sediment-starved conditions. Earth Surf. Dynam., 3, 291–309, 2016 https://doi.org/10.5194/esurf-3-291-2015, 2015.

Beer, A. R., Kirchner, J.W., and Turowski, J.M.: Graffiti for science – erosion painting reveals spatially variable erosivity of sediment-laden flows. Earth Surf. Dynam., 4, 885–894, 2016 https://doi.org/10.5194/esurf-4-885-2016, 2016.

Beer, A. R., Turowski, J.M., and Kirchner, J.W.: Spatial patterns of erosion in a bedrock gorge, J. Geophys Res-Earth, 122, 191–214, https://doi.org/10.1002/2016JF003850, 2017.

Chatanantavet, P., and Parker, G.: Physically based modeling of bedrock incision by abrasion, plucking, and macroabrasion, J. Geophys. Res., 114, F04018, https://doi.org/10.1029/2008JF001044, 2009

Chatanantavet, P., and Parker, G.: Experimental study of bedrock channel alluviation under varied sediment supply and hydraulic conditions, Water Resour. Res., 44, W12,446, https://doi.org/10.1029/2007WR006581, 2008

Cook, K.L, Turowski, J.M., and Hovius, N.: A demonstration of the importance of bedload transport for fluvial bedrock erosion and knickpoint propagation. Earth Surf. Proc. Land., 38, 683-695, https://doi.org/10.1002/esp.3313, 2013.

Cook, K.L., Whipple, K.X, Heimsath, A.M., and Hanks, T.C.: Rapid incision of the Colorado River in Glen Canyon – insights from channel profiles, local incision rates, and modelling of lithologic controls. Earth Surf. Proc. Land., https://doi.org/10.1002/esp.1790, 2009.

Czapiga, M.: Systematic Connectivity in Single Thread Meandering Alluvial Rivers: Statistical Generalization of Hydraulic Geometry. MSc thesis, University of Illinois at Urbana-Champaign, http://hdl.handle.net/2142/44498, 2009.

Ferguson, R.I., Sharma, B.P., Hodge, R.A., Hardy, R.J., and Warburton, J.: Bed load tracer mobility in a mixed bedrock/alluvial channel. J. Geophys. Res.-Earth, 122, 807-822, https://doi.org10.1002/2016JF003946, 2017.

Fernández, R.: Laboratory experiments on alluvial cover in mixed bedrock-alluvial meandering channels and on the formation and evolution of supraglacial meltwater meandering streams. PhD Thesis. University of Illinois at Urbana-Champaign. http://hdl.handle.net/2142/101494, 2018.

Fernández, R., Parker, G., and Stark, C.: Experiments on patterns of alluvial cover and bedrock erosion in a meandering channel. University of Illinois at Urbana-Champaign. https://doi.org/10.13012/B2-3044828_V1, 2019.

Finnegan, N. J., Sklar, L. S., and Fuller, T. K.: Interplay of sediment supply, river incision, and channel morphology revealed by the transient evolution of an experimental bedrock channel. J. Geophys. Res.-Earth, 112(3):1–17, https://doi.org/10.1029/2006JF000569, 2007.

Gasparini, N. M., Whipple, K. X., and Bras, R. L.: Predictions of steady state and transient landscape morphology using sediment-flux-dependent river incision models. J. Geophys. Res.-Earth, 112(3):1–20, https://doi.org/10.1029/2006JF000567, 2007

Gilbert, G.: Geology of the Henry Mountains. Technical report, U.S. Department of the Interior, 1877.

Hodge, R., and Hoey, T.B.: A Froude-scaled model of a bedrock-alluvial channel reach: 2. Sediment cover. J. Geophys. Res.-Earth, 121, 1597-1618, https://doi.org10.1002/2015JF003709, 2016.

Hodge, R., Hoey, T., Maniatis, T., and Lepretre, E.: Formation and erosion of sediment cover in an experimental bedrock-alluvial channel. Earth Surf. Proc. Land., 41, 1409-1420, https://doi.org/10.1002/esp.3924, 2016

Hodge, R., Hoey, T.B., and Sklar, L.: Bed load transport in bedrock rivers: The role of sediment cover in grain entrainment, translation, and deposition. J. Geophys. Res., 116, F04028, https://doi.org/10.1029/2011JF002032, 2011.

Inoue, T., Parker, G., and Stark. C.P.: Morphodynamics of a bedrock-alluvial meander bend that incises as it migrates outward: Approximate solution of permanent form. Earth Surf. Proc. Land., 42, 1342-1354, https://doi.org/10.1002/esp.4094, 2017.

Inoue, T., Iwasaki, T., Parker, G., Shimizu, Y., Izumi, N., Stark, C.P. and Funaki, J.: Numerical simulation of effects of sediment supply on bedrock channel morphology. J. Hydraul. Eng., 142(7), 04016014, https://doi.org /10.1061/(ASCE)HY.1943-7900.0001124, 2016.

Inoue, T., Izumi, N., Shimizu, Y., and Parker, G.: Interactions among alluvial cover, bed roughness, and incision rate in purely bedrock and alluvial-bedrock channel. J. Geophys. Res.-Earth, 119, 2123–2146 https://doi.org/10.1002/2014JF003133, 2014.

Johnson, J.P.: A surface roughness model for predicting alluvial cover and bed load transport rate in bedrock channels. J. Geophys. Res.-Earth, 119, 2147-2173, https://doi.org/10.1002/2013JF003000, 2014

Johnson, J. P., and Whipple, K.X.: Evaluating the controls of shear stress, sediment supply, alluvial cover, and channel morphology on experimental bedrock incision rate, J. Geophys. Res., 115, F02018, https://doi.org 10.1029/2009JF001335, 2010.

Johnson, J. P., and Whipple, K.X.: Feedbacks between erosion and sediment transport in experimental bedrock channels, Earth Surf. Proc. Land., 32, 1048–1062, https://doi.org/10.1002/esp.1471, 2007.

Johnson, K.N., and Finnegan, N. J.: A lithologic control on active meandering in bedrock channels. Geol. Soc. Am. Bull., 127(11/12), 1766-1776, https://doi.org/10.1130/B31184.1, 2015.

Lague, D.: Reduction of Long-Term Bedrock Incision Efficiency by Short-Term Alluvial Cover Intermittency. J. Geophys. Res.-Earth, 115, F2, F02011, https://doi.org/10.1029/2008JF001210, 2010.

Lamb, M. P., Dietrich, W.E., and Sklar, L.S.: A model for fluvial bedrock incision by impacting suspended and bedload sediment, J. Geophys. Res., 113, F03025, https://doi.org/10.1029/2007JF000915, 2008

Mishra, J., Inoue, T., Shimizu, Y., Sumner, T., and Nelson, J.M.: Consequences of abrading bed load on vertical and lateral erosion in a curved experimental channel. J. Geophys. Res.-Earth, 123, 3147-3161, https://doi.org/10.1029/2017JF004387, 2018.

Nelson, P.A., Bolla Pittaluga, M., and Seminara, G.: Finite amplitude bars in mixed bedrock-alluvial channels. J. Geophys. Res.-Earth. 119, 566-587, https://doi.org/10.1002/2013JF002957, 2014.

Nelson, P.A., and Seminara, G.: A theoretical framework for the morphodynamics of bedrock channels. Geophys. Res. Lett., 39, L06408, https://doi.org/10.1029/2011GL050806, 2012.

Otsu, N.: A Threshold Selection Method from Gray-Level Histograms. IEEE T. Sys. Man Cyb., 9(1), 62-66, 1979.

Sklar, L. S., and Dietrich, W. E.: The role of sediment in controlling steady-state bedrock channel slope: Implications of the saltation abrasion incision model. Geomorphology, 82, 58–83, https://doi.org/10.1016/j.geomorph.2005.08.019, 2006.

Sklar, L. S., and Dietrich, W.E.: A mechanistic model for river incision into bedrock by saltating bedload, Water Resour. Res., 40, W06301, https://doi.org/10.1029/2003WR002496, 2004.

Sklar, L. S., and Dietrich, W. E.: Sediment and rock strength controls on river incision into bedrock. Geology, 29(12), 1087-1090, https://doi.org/10.1130/0091-7613(2001)029<1087:SARSCO>2.0.CO;2, 2001.

Sklar, L.S., and Dietrich, W.E.: River longitudinal profiles and bedrock incision models: stream power and the influence of sediment supply. Rivers over rock: Fluvial processes in bedrock channels. Geophysical Monograph 107. American Geophysical Union, https://doi.org/10.1029/GM107p0237, 1998.

Turowski, J.M.: Alluvial cover controlling the width, slope and sinuosity of bedrock channels. Earth Surf. Dynam. 6:29-48, https://doi.org/10.5194/esurf-6-29-2018, 2018.

Turowski, J.M., and Hodge, R.: A probabilistic framework for the cover effect in bedrock erosion. Earth Surf. Dynam., 5, 311–330, https://doi.org/10.5194/esurf-5-311-2017, 2017.

Turowski, J. M., Hovius, N., Meng-Long, H., Lague, D., and Men-Chiang, C.: Distribution of erosion across bedrock channels. Earth Surf. Proc. Land., 33:353–363, https://doi.org/10.1002/esp.1559, 2008.

Turowski, J. M., Lague, D., and Hovius, N.: Cover effect in bedrock abrasion: A new derivation and its implications for the modeling of bedrock channel morphology. J. Geophys. Res., 112, F04006, https://doi.org/10.1029/2006JF000697, 2007.

Whipple, K. X., Hancock, G. S., and Anderson, R. S.: River incision into bedrock: Mechanics and relative efficacy of plucking, abrasion, and cavitation. Geol. Soc. Am. Bull., 112(3), 490–503, https://doi.org/ 10.1130/0016-7606(2000)112<490:RIIBMA>2.0.CO, 2000.

Zhang, L., Stark, C., Schumer, R., Kwang, J., Li, T., Fu, X., et al.: The advective-diffusive morphodynamics of mixed bedrock-alluvial rivers subjected to spatiotemporally varying sediment supply. J. Geophys. Res.-Earth, 123, 1731-1755, https://doi.org/10.1029/2017JF004431, 2018.

Zhang, L., Parker, G., Stark, C. P., Inoue, T., Viparelli, E., Fu, X., and Izumi, N.: Macro-roughness model of bedrock alluvial river morphodynamics. Earth Surf. Dynam., 3, 113–138, https://doi.org/10.5194/esurf-3-113-2015 , 2015.

Earth Surf. Dynam. Discuss., https://doi.org/10.5194/esurf-2019-8
Manuscript under review for journal Earth Surf. Dynam.
Discussion started: 27 February 2019

Table 1 Hydraulic parameters common to all experimental conditions

Parameter		Value
Flow discharge	Q [m^3/s]	0.0123
Channel width	B [m]	0.60
Centerline depth	H [m]	0.11
Reach-averaged velocity	U [m/s]	0.19
Hydraulic radius	R_h [m]	0.08
Froude number	F_r [-]	0.18

Earth Surf. Dynam. Discuss., https://doi.org/10.5194/esurf-2019-8
Manuscript under review for journal Earth Surf. Dynam.
Discussion started: 27 February 2019

Table 2 Experiment parameters specific to each run.

Run ID	Reach-averaged fraction of cover	Water Temperature	Average bed load transport rate	Water surface slope, middle bend	Water surface slope, entire flume	Kinematic viscosity	Reynolds Number
[-]	p_c [-]	T [°C]	q_{bs} [g/s]	S [mm/m]	S [mm/m]	[mm^2/s]	R_e [-]
pc00	0.00	24	0.00	0.99	0.68	0.9131	16,328
pc19	0.19	20	0.08	0.97	0.79	1.0034	14,859
pc27	0.27	24	0.25	0.99	0.75	0.9131	16,328
pc38	0.38	27	0.55	1.14	0.88	0.8539	17,460
pc46	0.46	21	1.47	1.19	1.01	0.9795	15,221
pc54	0.54	22	- [a]	1.03[b]	0.79	0.9565	15,587
pc72	0.72	27	4.50	1.26[b]	0.97	0.8539	17,460
pc79	0.79	24	5.60	1.26[b]	0.97	0.9131	16,328

[a] Bed load transport rate not measured for this condition.

[b] Slopes estimated based on the average ratio between middle bend slopes to flume slopes of previous five experimental conditions.

Earth Surf. Dynam. Discuss., https://doi.org/10.5194/esurf-2019-8
Manuscript under review for journal Earth Surf. Dynam.
Discussion started: 27 February 2019

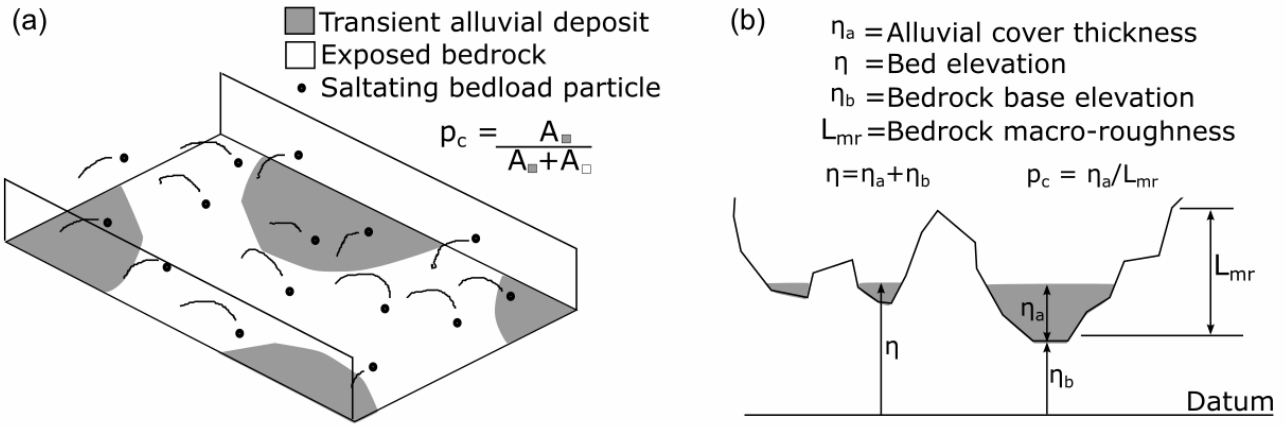

Figure 1. Schematic representations of (a) the fraction of exposed bedrock showing surface areal cover (Sklar and Dietrich, 2004) and (b) a cross section illustrating filling of a rough bedrock surface with alluvium (Zhang et al., 2015).

Earth Surf. Dynam. Discuss., https://doi.org/10.5194/esurf-2019-8
Manuscript under review for journal Earth Surf. Dynam.
Discussion started: 27 February 2019

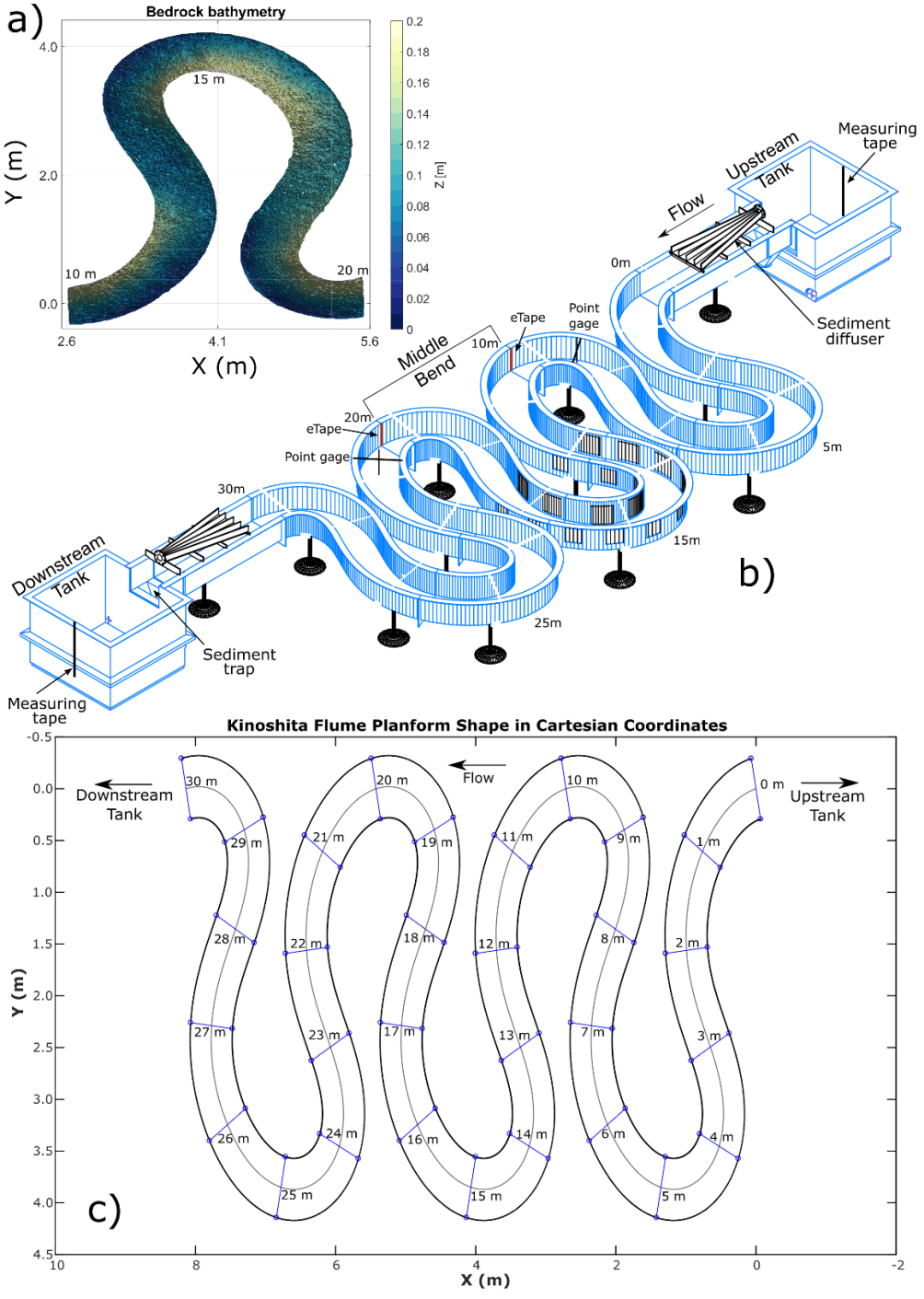

Figure 2: a) Bedrock bathymetry built inside the Kinoshita flume. Streamwise locations 10m, 15m and 20m are indicated; b) 3D rendering of Kinoshita flume showing location of tank measuring tapes, point gages, eTapes, sediment trap and sediment diffuser, flow direction, and middle bend where all measurements were made; c) Kinoshita shape with streamwise stations indicated. Flow direction from right to left.

Earth Surf. Dynam. Discuss., https://doi.org/10.5194/esurf-2019-8
Manuscript under review for journal Earth Surf. Dynam.
Discussion started: 27 February 2019

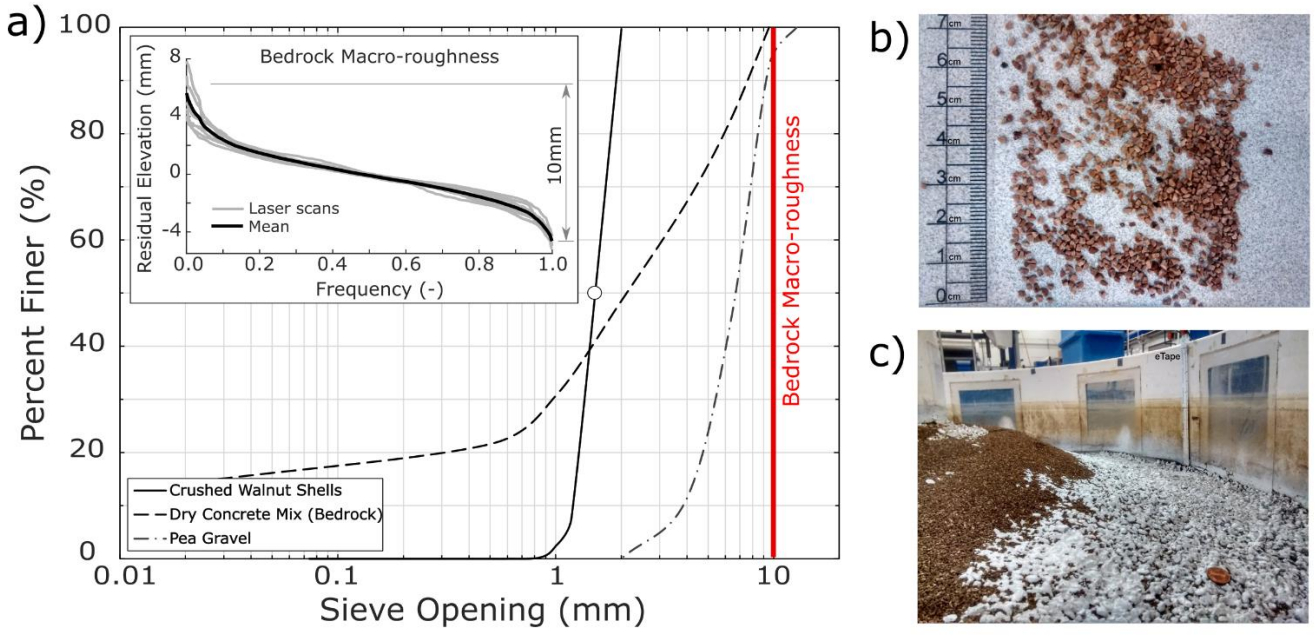

Figure 3. a) Grain size distributions for the alluvium (crushed walnut shells), dry concrete mix used to build the bedrock, and the pea gravel underlying the bedrock basement. Insert shows residual elevations of as-built bedrock bed, measured with laser scans at different cross sections inside the Kinoshita flume. Mean macro-roughness (~10mm) is also indicated in the main plot; b) Image of crushed walnut shells with ruler for scale; and c) Bedrock bed partially covered with alluvium inside the Kinoshita flume.

Earth Surf. Dynam. Discuss., https://doi.org/10.5194/esurf-2019-8
Manuscript under review for journal Earth Surf. Dynam.
Discussion started: 27 February 2019

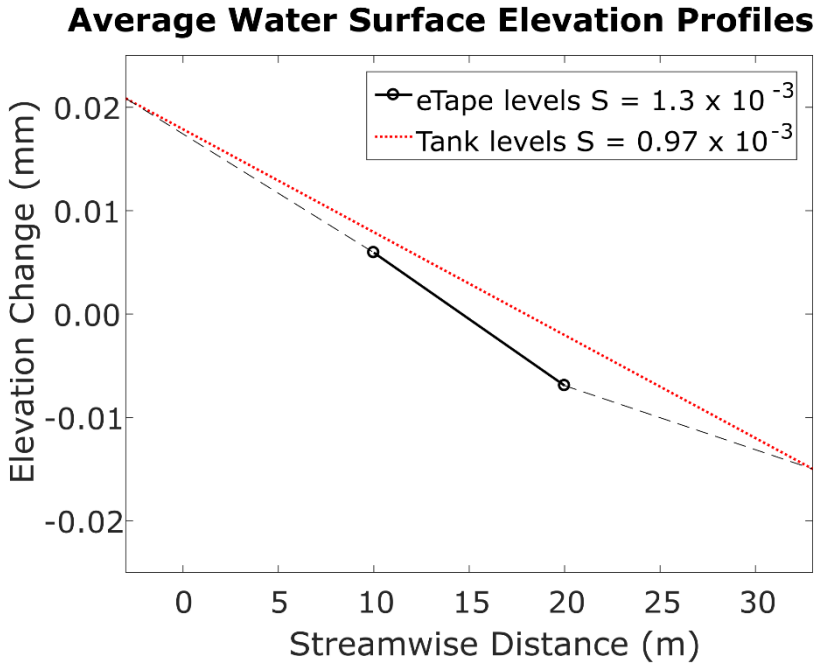

Figure 4 Average water surface elevation profiles and corresponding slopes based on the eTape readings and the levels measured in the upstream and downstream tanks for Run pc79.

Earth Surf. Dynam. Discuss., https://doi.org/10.5194/esurf-2019-8
Manuscript under review for journal Earth Surf. Dynam.
Discussion started: 27 February 2019

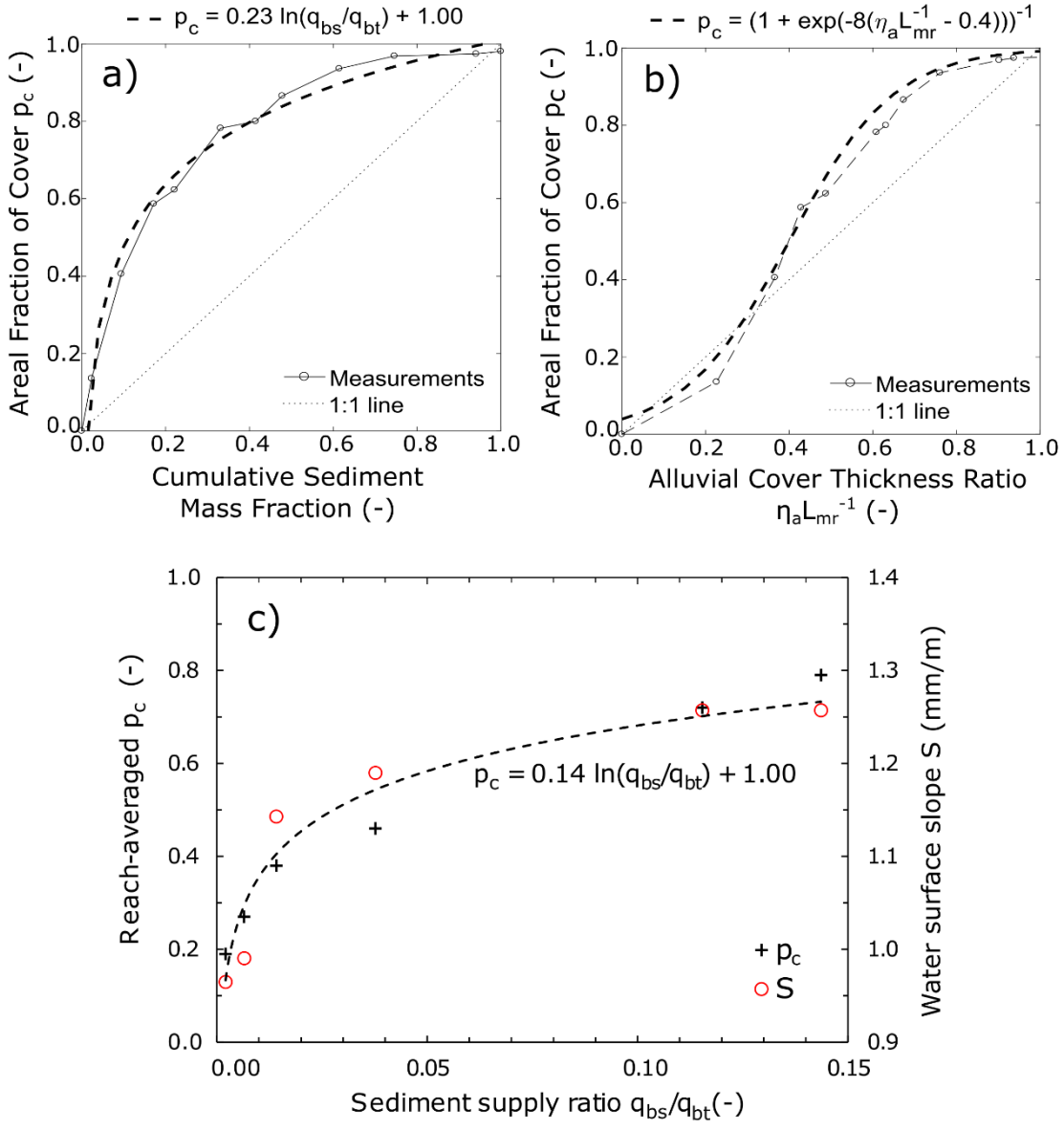

Figure 5 a) Relation between areal fraction of alluvial cover and sediment supply ratio for bedrock slab; b) Relation between areal fraction of alluvial cover and the ratio between alluvial thickness and bedrock macro-roughness for bedrock slab; c) Relation between reach-averaged areal fraction of alluvial cover and sediment supply ratio for Kinoshita flume and corresponding water surface slopes as a function of sediment supply ratio.

Earth Surf. Dynam. Discuss., https://doi.org/10.5194/esurf-2019-8
Manuscript under review for journal Earth Surf. Dynam.
Discussion started: 27 February 2019

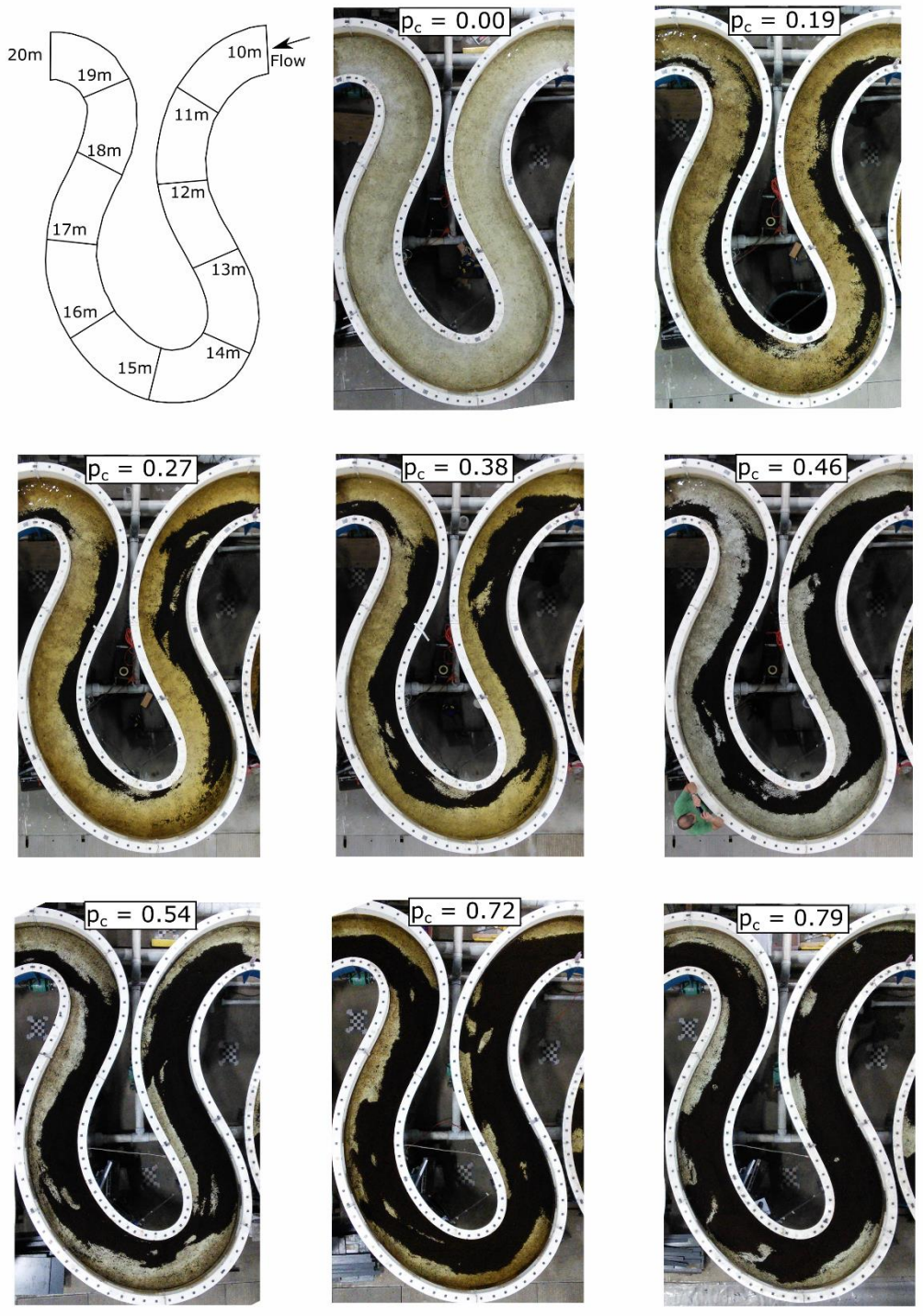

Figure 6 Images of the middle bend of the Kinoshita flume corresponding to an instant during each of the eight different areal alluvial cover conditions. Volume of sediment in the system grows from top to bottom and left to right. Diagram included at the top-left shows flow direction and contains cross sections indicating the streamwise locations along the middle bend of the flume.

Earth Surf. Dynam. Discuss., https://doi.org/10.5194/esurf-2019-8
Manuscript under review for journal Earth Surf. Dynam.
Discussion started: 27 February 2019

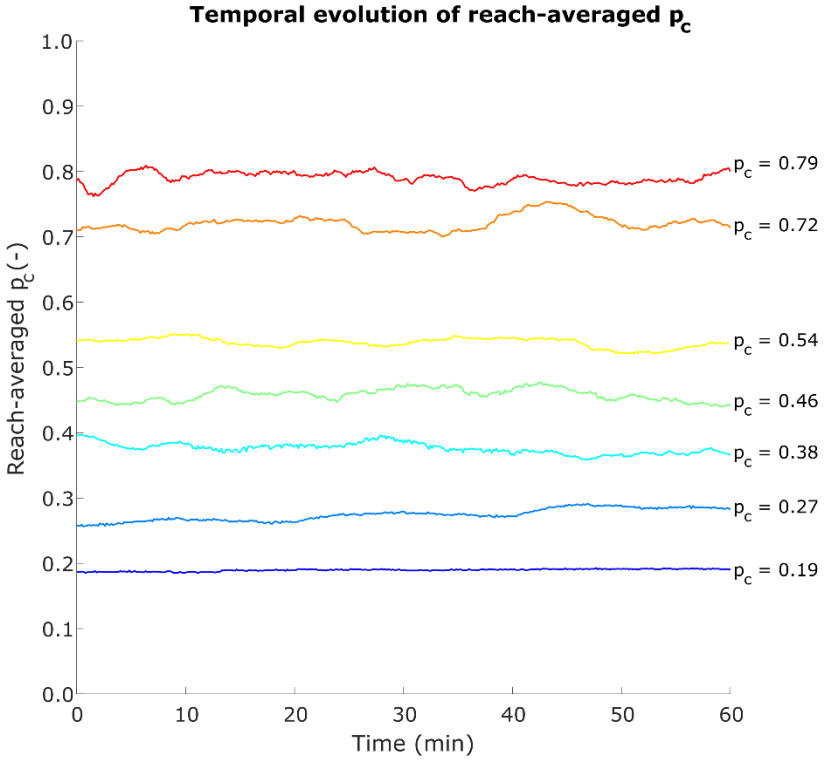

Figure 7 Temporal evolution of reach-averaged areal fraction of alluvial cover for all experimental conditions that had alluvium.

Earth Surf. Dynam. Discuss., https://doi.org/10.5194/esurf-2019-8
Manuscript under review for journal Earth Surf. Dynam.
Discussion started: 27 February 2019

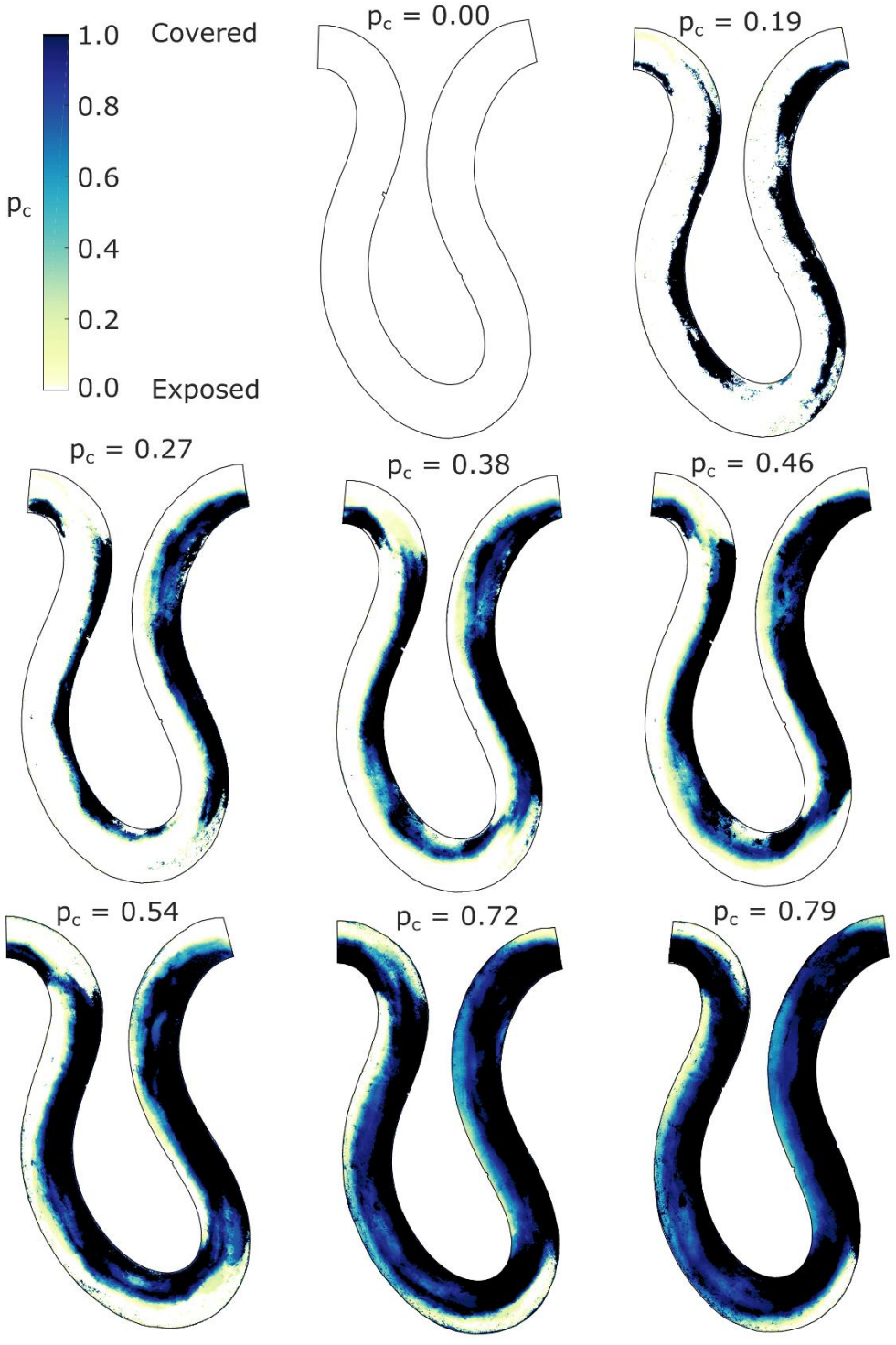

Figure 8 Maps of spatiotemporal averages of areal fraction of alluvial cover for all experimental conditions.

Earth Surf. Dynam. Discuss., https://doi.org/10.5194/esurf-2019-8
Manuscript under review for journal Earth Surf. Dynam.
Discussion started: 27 February 2019

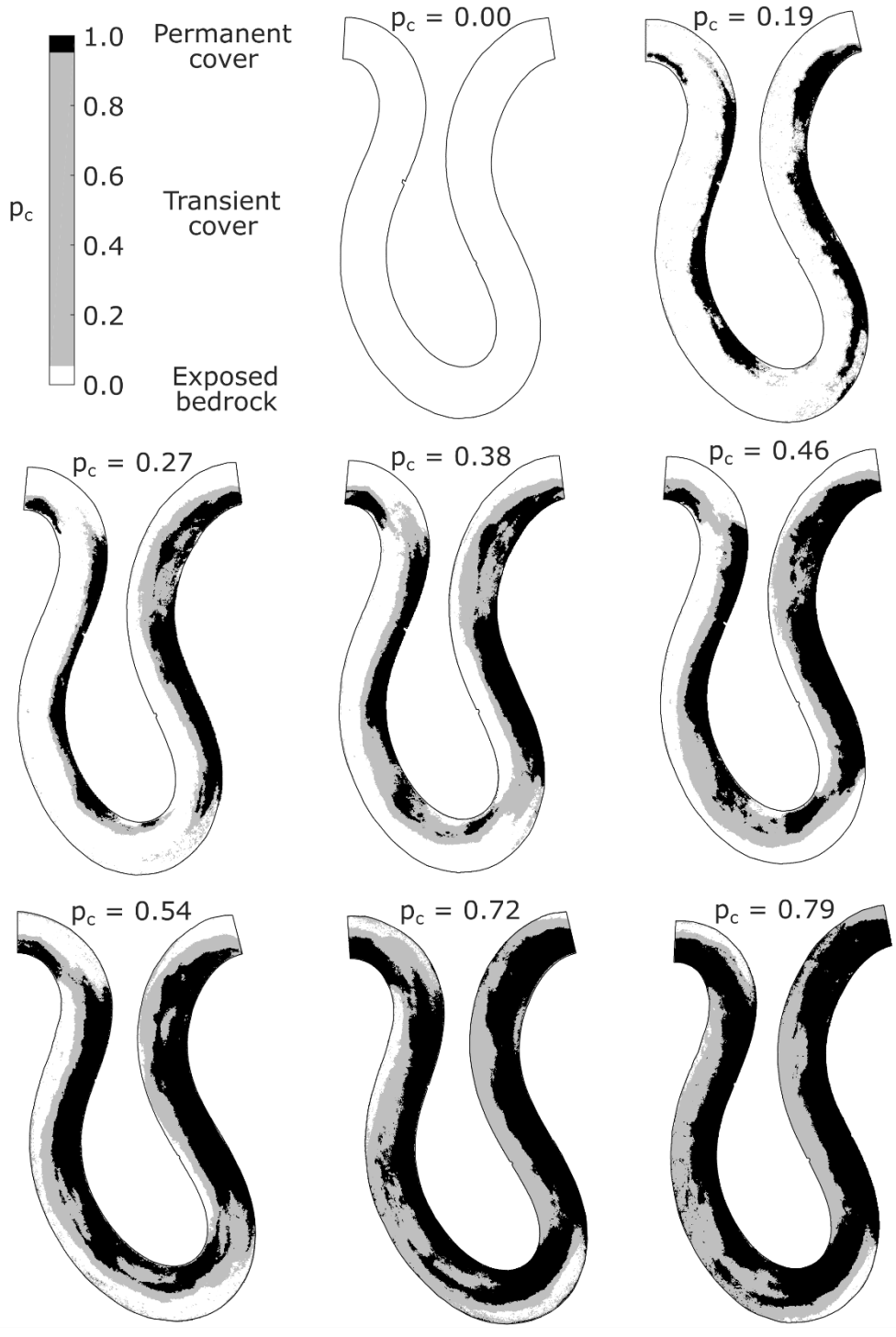

Figure 9 Maps showing regions with permanent alluvial cover, transient alluvial cover and permanently exposed bedrock for all experimental conditions.

Earth Surf. Dynam. Discuss., https://doi.org/10.5194/esurf-2019-8
Manuscript under review for journal Earth Surf. Dynam.
Discussion started: 27 February 2019

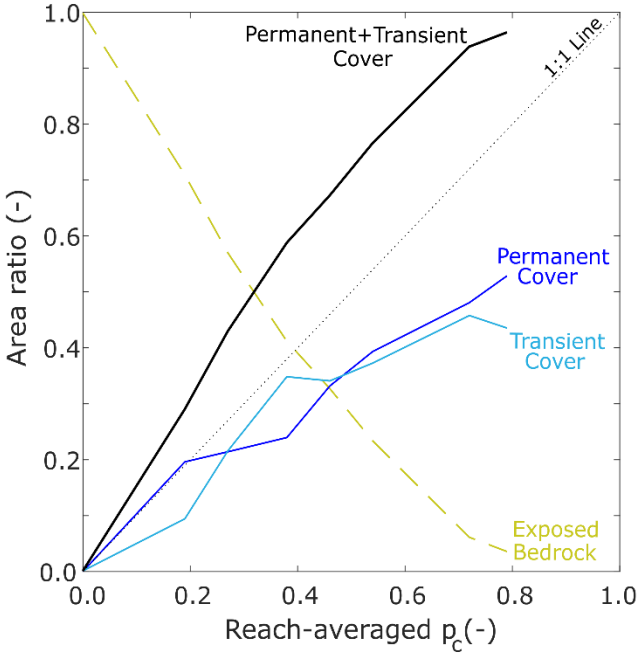

Figure 10 Reach-averaged area ratios of permanently exposed bedrock, transient alluvial cover, permanent alluvial cover, and permanent + transient alluvial cover as a function of reach-averaged areal cover fraction.

Earth Surf. Dynam. Discuss., https://doi.org/10.5194/esurf-2019-8
Manuscript under review for journal Earth Surf. Dynam.
Discussion started: 27 February 2019

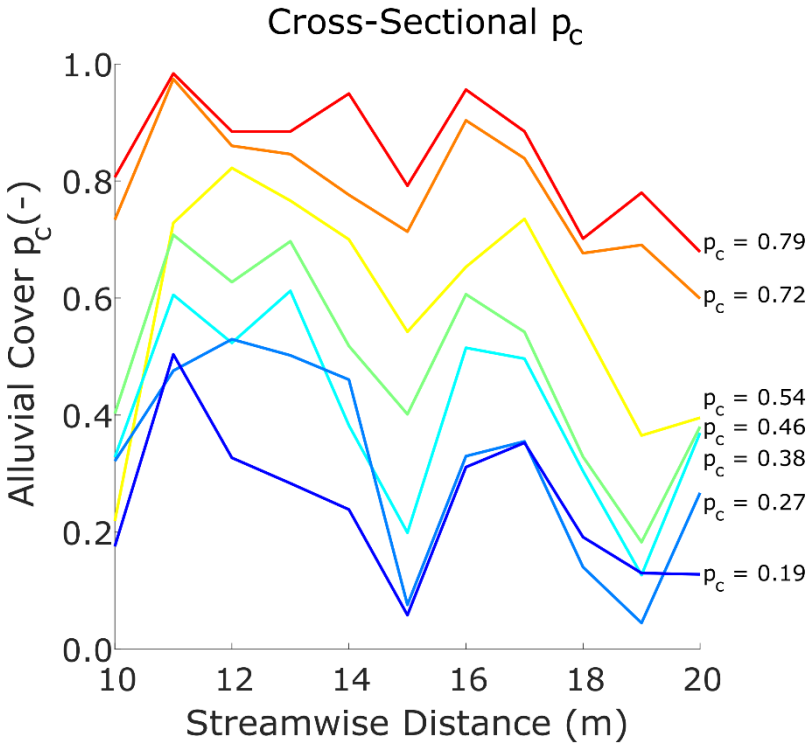

Figure 11 Cross-sectional averages of areal fraction of alluvial cover for all experimental runs. Local values were extracted every meter between streamwise locations 10 m and 20 m. The legend indicates the corresponding reach-averaged values.

Earth Surf. Dynam. Discuss., https://doi.org/10.5194/esurf-2019-8
Manuscript under review for journal Earth Surf. Dynam.
Discussion started: 27 February 2019

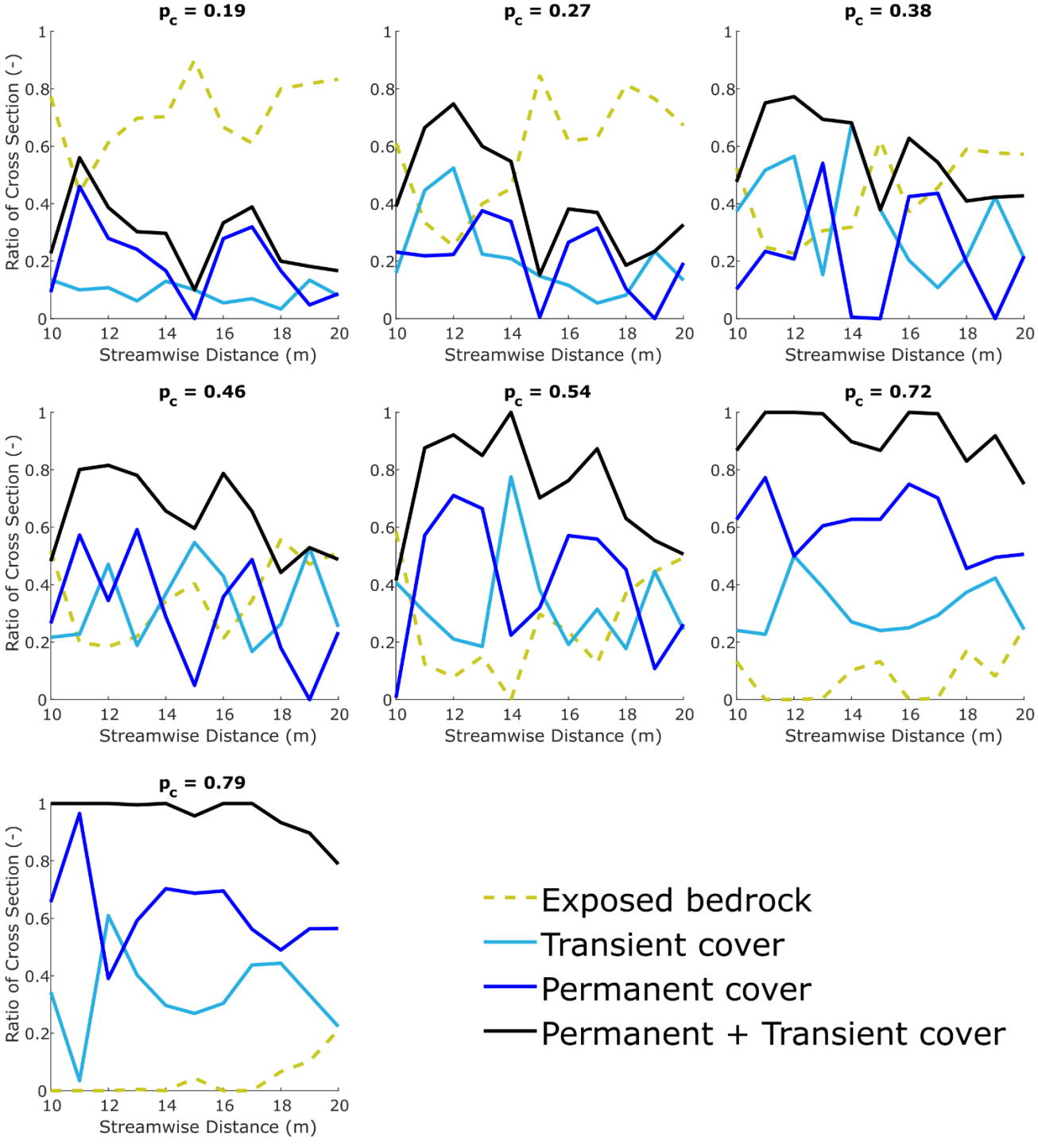

Figure 12 Cross-sectionally-averaged ratios of permanently exposed bedrock, transient alluvial cover, permanent (static) alluvial cover, and static + transient alluvial cover for all experimental conditions.

Earth Surf. Dynam. Discuss., https://doi.org/10.5194/esurf-2019-8
Manuscript under review for journal Earth Surf. Dynam.
Discussion started: 27 February 2019

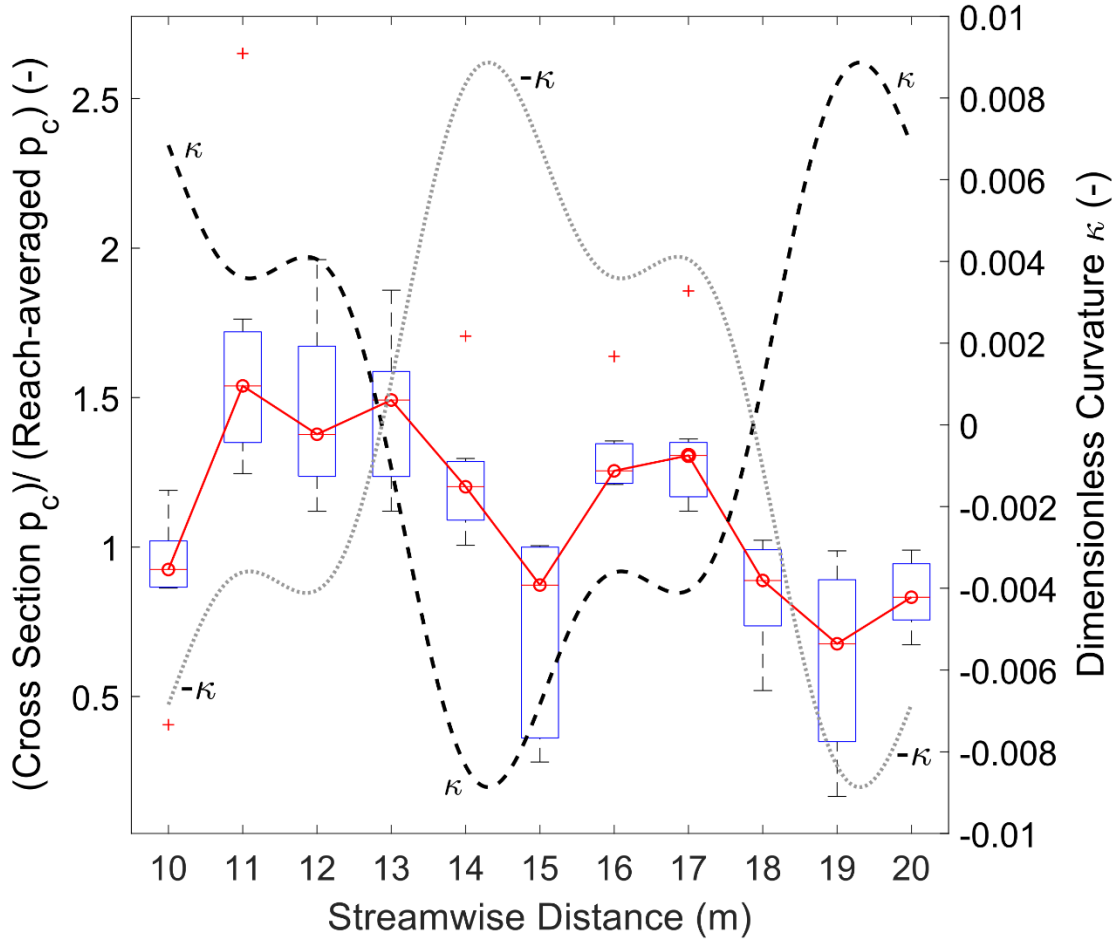

Figure 13 Boxplots of normalized cross-sectionally-averaged areal fraction of alluvial cover in the middle bend of the Kinoshita flume. The dimensionless curvature of the flume κ and its negative value - κ are plotted to better show the salient trends.

Earth Surf. Dynam. Discuss., https://doi.org/10.5194/esurf-2019-8
Manuscript under review for journal Earth Surf. Dynam.
Discussion started: 27 February 2019

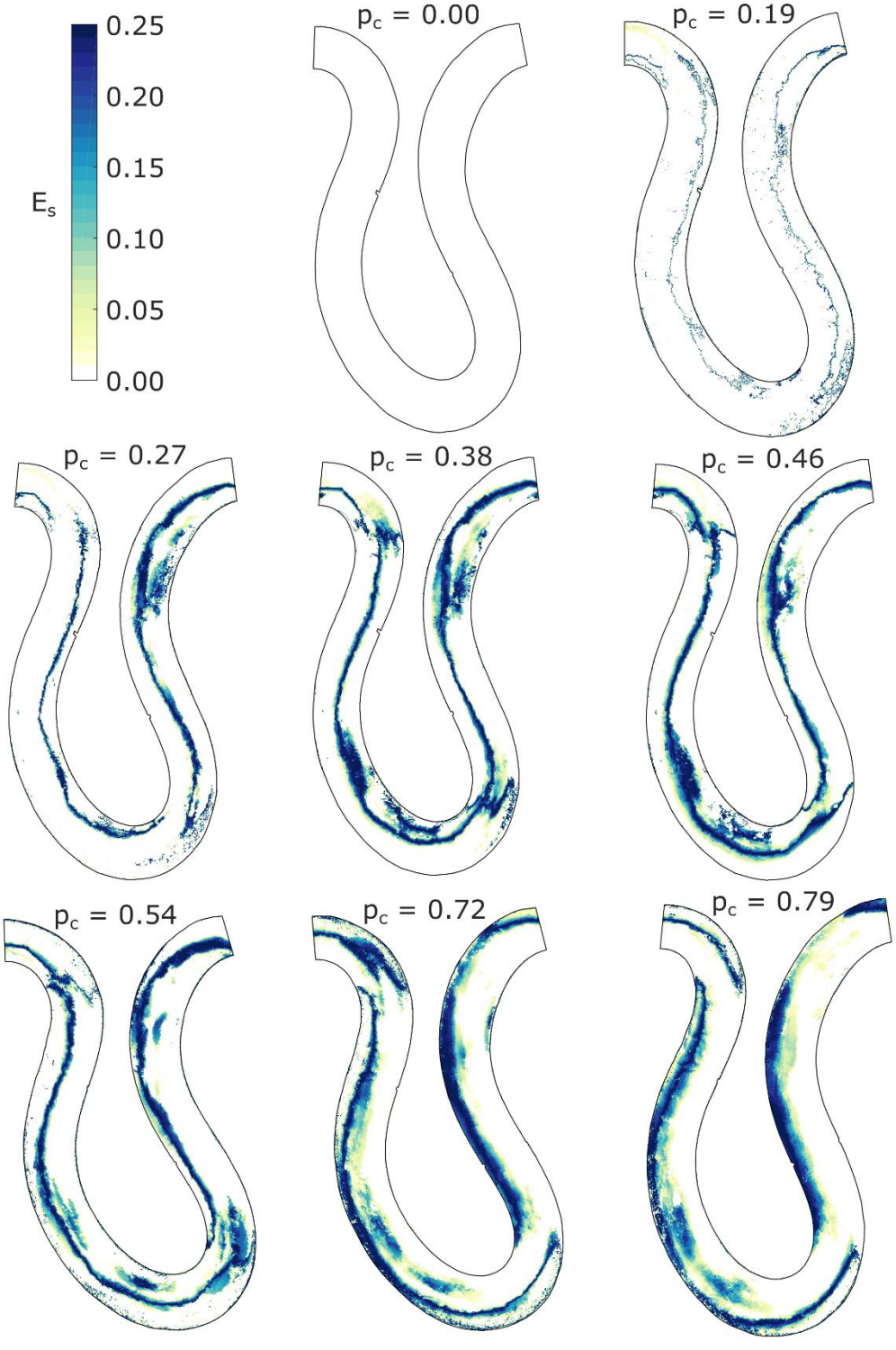

Figure 14 Maps of spatiotemporally-averaged erosion potential for all experimental conditions.

Earth Surf. Dynam. Discuss., https://doi.org/10.5194/esurf-2019-8
Manuscript under review for journal Earth Surf. Dynam.
Discussion started: 27 February 2019

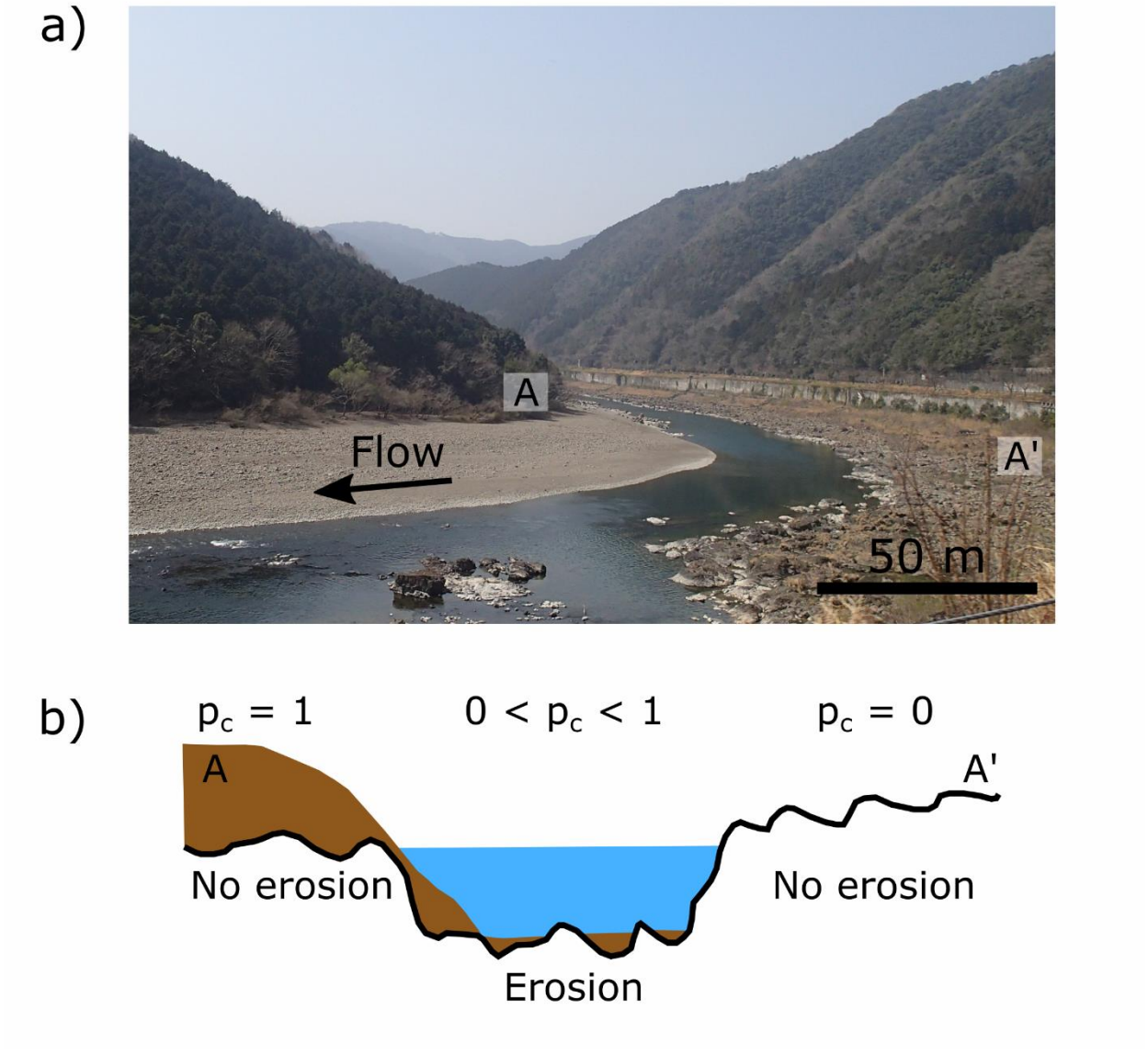

Figure 15 a) Image of a reach of the Shimanto River, Shikoku, Japan showing partial cover with alluvium. b) Sketch of cross section A-A' (with strong vertical exaggeration) indicating inferred regions of erosion and no erosion.

Earth Surf. Dynam. Discuss., https://doi.org/10.5194/esurf-2019-8
Manuscript under review for journal Earth Surf. Dynam.
Discussion started: 27 February 2019

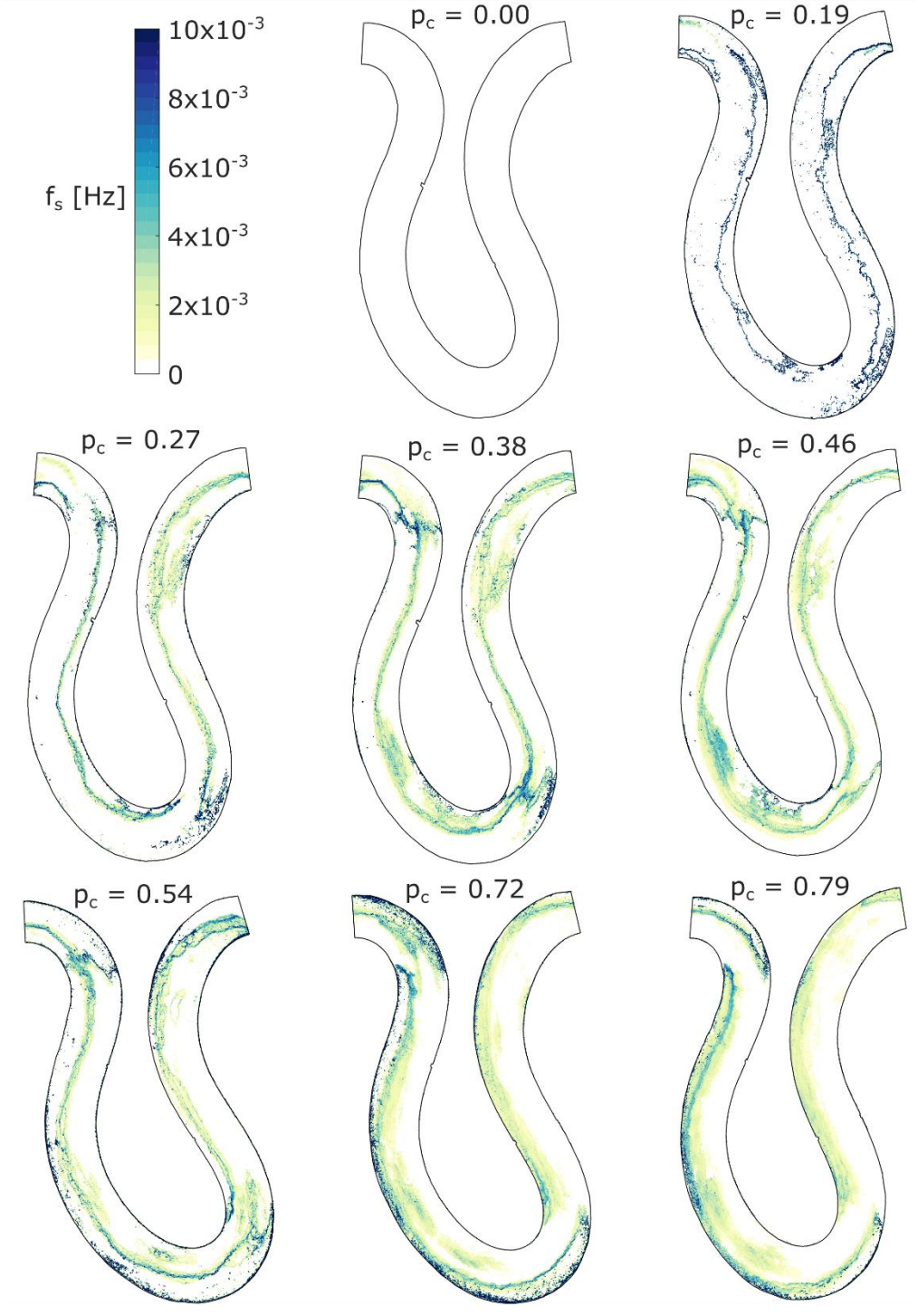

Figure 16 Maps of frequency of strikes for all experimental conditions. Frequency shown is based on number of images. Dividing the values by 10 s which is the time between images will give the actual frequency in Hz.

Earth Surf. Dynam. Discuss., https://doi.org/10.5194/esurf-2019-8
Manuscript under review for journal Earth Surf. Dynam.
Discussion started: 27 February 2019

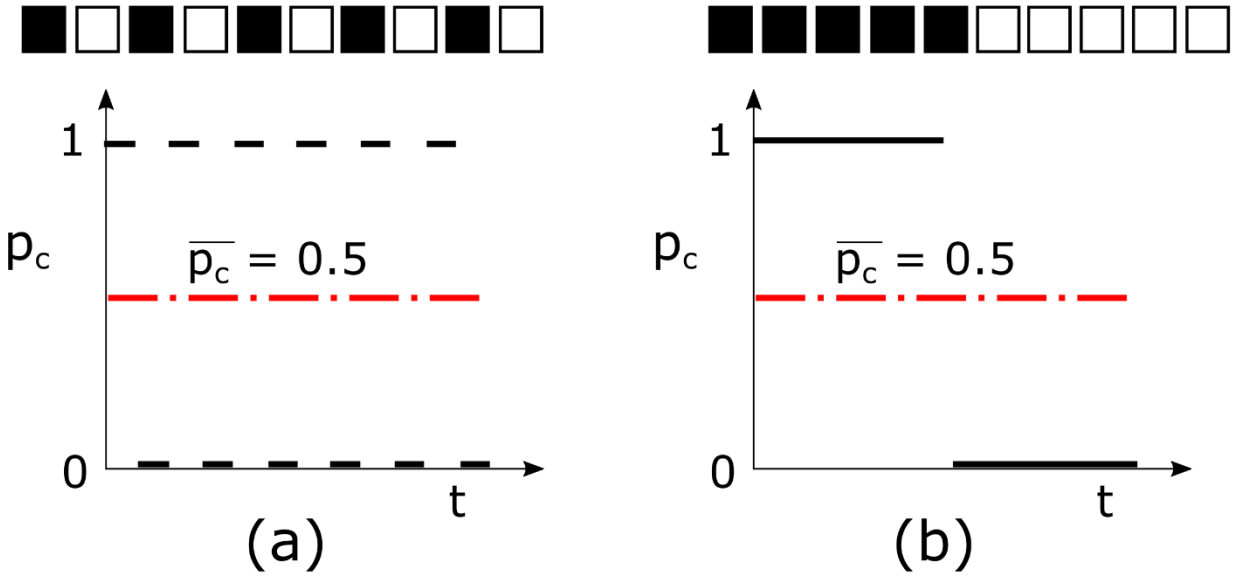

Figure 17 Simple example showing that temporal averages alone of the areal cover fraction of alluvial cover are insufficient to quantify bedrock incision. Bed conditions (a) and (b) have the same average cover but (a) would experience more erosion than (b) due to a greater frequency of fluctuations in alluvial cover.